

1980

Non-linear behavior of unbraced two-bay reinforced concrete frames

Mehdi Shadyab
Portland State University

Follow this and additional works at: https://pdxscholar.library.pdx.edu/open_access_etds



Part of the [Engineering Science and Materials Commons](#)

Let us know how access to this document benefits you.

Recommended Citation

Shadyab, Mehdi, "Non-linear behavior of unbraced two-bay reinforced concrete frames" (1980).
Dissertations and Theses. Paper 2974.
<https://doi.org/10.15760/etd.2969>

This Thesis is brought to you for free and open access. It has been accepted for inclusion in Dissertations and Theses by an authorized administrator of PDXScholar. Please contact us if we can make this document more accessible: pdxscholar@pdx.edu.

AN ABSTRACT OF THE THESIS OF Mehdi Shadyab for the Master of Science
in Applied Science presented November 20, 1980.

Title: Non-Linear Behavior of Unbraced Two-bay Reinforced Concrete
Frames

APPROVED BY MEMBERS OF THE THESIS COMMITTEE:

[REDACTED]
Franz N. Rad, Chairman

[REDACTED]
Wendelin H. Mueller, III

[REDACTED]
Thomas J. Gavin

[REDACTED]
Selmo Tauber

In this investigation, the primary objective was to study the non-linear behavior of unbraced two-bay concrete frames and to determine the extent to which ultimate load theory or limit design can be applied to these structures. The frame behavior was investigated analytically by two methods. In the first method the frame stability equation was derived assuming that members of the frame possess an elasto-plastic moment-curvature relationship. This stability analysis was also carried out by another model consisting of a column attached to a linear spring and carrying the total frame load. The second method was through a computer program which took material and geometric nonlinearities of concrete frames into account. A model concrete frame, with a scale factor of approximately one-third was considered. Variable parameters

were loading condition, column reinforcement ratio, and beam to column load ratio. For each frame, the gravity loads were increased proportionally until 75% of the frame ultimate capacity under gravity loads was reached. Then; while these gravity loads were held constant, lateral load was applied and increased to failure. The overall geometry, 21-in high columns and 84-in long beam, were kept the same for all of model frames investigated. The computer study and the stability model analysis indicated that all frames remained stable until four plastic hinges (two in each bay) formed, thus producing a combined sway mechanism. Based on the scope of this study, it appears that limit design may be employed for unbraced reinforced concrete structures.

NON-LINEAR BEHAVIOR OF UNBRACED TWO-BAY
REINFORCED CONCRETE FRAMES

by

MEHDI SHADYAB

A thesis submitted in partial fulfillment of the
requirements for the degree of

MASTER OF SCIENCE
in
APPLIED SCIENCE

Portland State University

1980

TO THE OFFICE OF GRADUATE STUDIES AND RESEARCH:

The members of the Committee approve the thesis of Mehdi Shadyab presented November 20, 1980.

[Redacted]

Franz N. Rad, Chairman

[Redacted]

Wendelin H. Mueller, III

[Redacted]

Thomas J. Gavin

[Redacted]

Selmo Tauber

APPROVED:

[Redacted]

Franz N. Rad, Head, CIVIL-Structural Engineering

[Redacted]

Stanley E. Rauch, Dean of Graduate Studies and Research

TO MY PARENTS

ACKNOWLEDGMENTS

This research was conducted under the supervision of Dr. Franz N. Rad. The author wishes to express his grateful appreciation and gratitude to Dr. Rad for his continued leadership, priceless advice and encouragement throughout this investigation.

The author is indebted to the other members of his thesis committee, Dr. Wendelin Mueller, Dr. Selmo Tauber and Mr. Tom Gavin for their helpful comments and suggestions.

Thanks is due to the Division of Engineering and Applied Science, especially Civil-Structural Engineering. The help of the Computer Center staff at Portland State University, especially Mr. Wes Brenner and Mr. Dave Dinucci is also acknowledged and appreciated. Special thanks are due to Mrs. Donna Mikulic for the fine job she did in typing this thesis.

Finally, the author wishes to acknowledge heartfelt gratitude to his parents and his sisters for their encouragement, love and understanding throughout the author's graduate work.

TABLE OF CONTENTS

	PAGE
ACKNOWLEDGMENTS.....	iv
LIST OF TABLES.....	vii
LIST OF FIGURES.....	viii
CHAPTER	
I INTRODUCTION.....	1
1.1 General.....	1
1.2 Objective.....	3
1.3 Organization.....	3
II MODELING CONSIDERATIONS.....	4
2.1 General.....	4
2.2 The Model Frame.....	4
2.3 Description of the Types of Frame Failure.....	10
2.4 Loading of the Prototype v.s. Model Frames.....	13
2.4.1 Frame Loading.....	13
2.4.2 Column Strength.....	13
2.4.3 Beam Strength.....	15
2.4.4 The Structural Analysis.....	17
III ELASTO-PLASTIC MODEL.....	21
3.1 General.....	21
3.2 Frame Loading, Assumptions, and Notation.....	21
3.3 Condition of the Frame at the First Hinge.....	25
3.4 Condition of the Frame After the First Hinge.....	27
3.4.1 Shear Distribution by Using a Spring Model.....	28

3.4.2	Shear Distribution by Yura's Method.....	28
3.5	Condition of the Frame when the Second Hinges Form at (K) and (M).....	31
3.6	The Inelastic Buckling Load by Bolton's Method.....	40
3.7	Elastic Instability of the Frame.....	43
3.7.1	λ for Exterior Columns.....	45
3.7.2	λ for Interior Column.....	48
3.8	Elastic Stability Equations for Multi-Bay Frames.....	50
3.9	Stability Domains Defined by the Elasto- Plastic Analysis.....	51
3.10	Comparison of Inelastic Stability Equation of Two-Bay Frames with Single-Bay Frames.....	55
IV	COMPUTER ANALYSIS.....	57
4.1	General.....	57
4.2	Description of the Computer Program.....	57
4.3	Parametric Study of the Model Frame.....	58
4.3.1	Frame Description.....	58
4.3.2	Design of Beams.....	60
4.3.3	Design of the Columns.....	62
4.3.4	Procedure and Computer Results.....	66
V	COMPARISON OF RESULTS BY TWO METHODS.....	73
5.1	General.....	73
5.2	Computer Results vs. Stability Domain Analysis.....	73
5.3	Summary of Results.....	83
VI	SUMMARY, CONCLUSIONS AND RECOMMENDATIONS.....	84
	REFERENCES	87

LIST OF TABLES

TABLE	PAGE
2.1 Comparison of Section Properties for the Model and the Prototype.....	16
2.2 The Relation Between Uniform and Concentrated Loads.....	20
3.1 The Effective Exterior and Interior Column Length Factor, by Exact Solution.....	49
3.2 The Elastic Stability Equation for Frames with Different Number of Bays.....	53
4.1 Q/P', Q/P, Q/T Ratios for Various Number of Stories, n.....	59
4.2 The Summary of Beam Sections.....	63
4.3 The Summary of Column Sections, $\rho_g = 2\%$	67
4.4 The Summary of Column Sections, $\rho_g = 8\%$	68
5.1 Summary of Computer Results for $\rho_g = 2\%$	74
5.2 Summary of Computer Results for $\rho_g = 8\%$	75
5.3 Comparison with Stability Domain Analysis $\rho_g = 2\%$	80
5.4 Comparison with Stability Domain Analysis $\rho_g = 8\%$	81

LIST OF FIGURES

FIGURE		PAGE
2.1	A Multi-Story Unbraced Concrete Frame.....	5
2.2	An Interior Panel.....	6
2.3	The Reduced Model Frame.....	6
2.4	Two Extreme Conditions.....	8
2.5	Example of a 5-Story Building at Two Extreme Conditions.	9
2.6	Types of Frame Failure.....	11
2.7	A Multi-Story Frame.....	14
2.8	An Interior Bay.....	14
3.1	The Reduced Model Frame.....	22
3.2	Loads and Moments at the First Hinge.....	26
3.3	Loads and Deflected Shape at the First Hinge.....	26
3.4	Spring Model and the Shear Distribution Caused by Lateral Load.....	29
3.5	Shear Distribution by Using a Spring Model.....	30
3.6a	Horizontal Shear Distribution After the First Hinges Due to P- Δ Effect Only.....	32
3.6b	Gravity and the Lateral Loads and the Horizontal Shear Distribution After the First Hinge.....	33
3.7	Loads, Moments and the Deflected Shape Caused by the Additional Lateral Load H_2 and Deflection Δ_2	34
3.8	The Stability Model.....	41
3.9	The Elastic Stability Equation.....	44
3.10	The Elastic Stability Equation.....	52

FIGURE		PAGE
3.11	The Stability Domains.....	54
3.12	Stability Domains for One and Two-Bay Frames.....	56
4.1	Lateral Load-Moment curves, $n = 3$ and 9	70
4.2	Lateral Load-Moment Curves, $n = 20$ and 30	71
5.1	Moment Redistribution Curves, $n = 3-9$	76
5.2	Moment Redistribution Curve, $n = 3-30$	78
5.3	The Stability Domains, $n = 3, 9$	79
5.4	The Stability Domains, $n = 20, 30$	82

CHAPTER I

INTRODUCTION

1.1 GENERAL

The inelastic behavior of reinforced concrete structures has been recognized for several decades (1,2), and the related research which spans over half a century (3) have clarified a number of important problems. However, despite the fact that there are some available theoretical and experimental data, the adoption of inelasticity concept in structural design of reinforced concrete remains elusive. Conventionally, the analyses of indeterminate reinforced concrete structures has been based on elastic method. The elastic method consists of determining the bending moments shear and axial thrusts by assuming that the structure is perfectly elastic, i.e., the material's stress-strain relationship varies linearly.

Since 1963, the American Concrete Institute (4), through the use of Ultimate Strength Design (USD), has allowed designing individual members and sections by recognizing their inelastic response, while the elastic structure is assumed to determine the moments and forces. In USD, the required strength to resist loads is found by multiplying the service loads by load factors, corresponding to the type of loading conditions. These load factors for a number of loading combinations have been determined based on the probability of the combination occurring and on the safety of the structure. The USD method is also used by codes of practice in several other countries such as Great Britain and the Soviet Union (5,6).

The application of ultimate load theory to structural design started as early as 1914 (7,8). This theory, in design of steel frames identified by "plastic design," utilizes the distribution of bending moment as well as the strength of a cross section beyond the elastic limit. Correspondingly, the ultimate load theory, which in reinforced concrete is referred to by "limit design," utilizes the redistribution of elastic moments in structures beyond the elastic limit. However, since reinforced concrete does not have the same ductility characteristics as structural steel there are some inconsistencies and unresolved problems regarding its response beyond the elastic range. Excessive cracks and deformation beyond the elastic range under service loads is another reason why the application of limit design in reinforced concrete has not been widely accepted. Nevertheless, due to the inelastic behavior of reinforced concrete members beyond the elastic state (26), the present standards allow a certain deviation from the elastic theory.

A 10% moment redistribution was permitted in the 1963 ACI code. The present ACI code (4) allows up to 20% moment redistribution depending on the reinforcement ratio (23). This figure is 15% in the 1972 CEB recommendation (9), 30% in the Soviet (10), 30% in the British (5), and up to 67% in the Danish standards (11).

Finally, limit design is preferred over the conventional elastic theory because of the following reasons:

1. the real properties of materials are considered (inelastic phenomenon),
2. in indeterminate structures as a section reaches its yield

- point, the structure will not collapse,
3. the reserved strength, beyond the elastic point to failure, is usually considerable, and
 4. reduction of negative moments reduces the steel concentration.

1.2 OBJECTIVE

The general objective of this investigation is to determine the applicability of limit design to multistory multibay unbraced concrete frames. The primary objective is to study the behavior of such frames under gravity and gravity plus lateral loading for the following conditions:

- (a) as the loading increases
- (b) as the relative flexural stiffness of the columns and beams varies
- (c) as the beam to column load ratio increases
- (d) as the reinforcement ratio varies

This investigation is carried out using two analytical techniques.

1.3 ORGANIZATION

The remaining part of this thesis is divided into five chapters. In Chapter II, the modeling consideration is discussed. In Chapter III, analytical treatment of frames using the mathematical solution of an elasto-plastic stability model frame is discussed.

The computer analysis of these model frames, using a computer program which takes material and geometry nonlinearities into account, is discussed in Chapter IV. Chapter V discusses the comparison of the two methods of analysis used for selected model frames, and finally Chapter VI includes the summary and conclusions of this study, along with some recommendations for future research.

CHAPTER II

MODELING CONSIDERATIONS

2.1 GENERAL

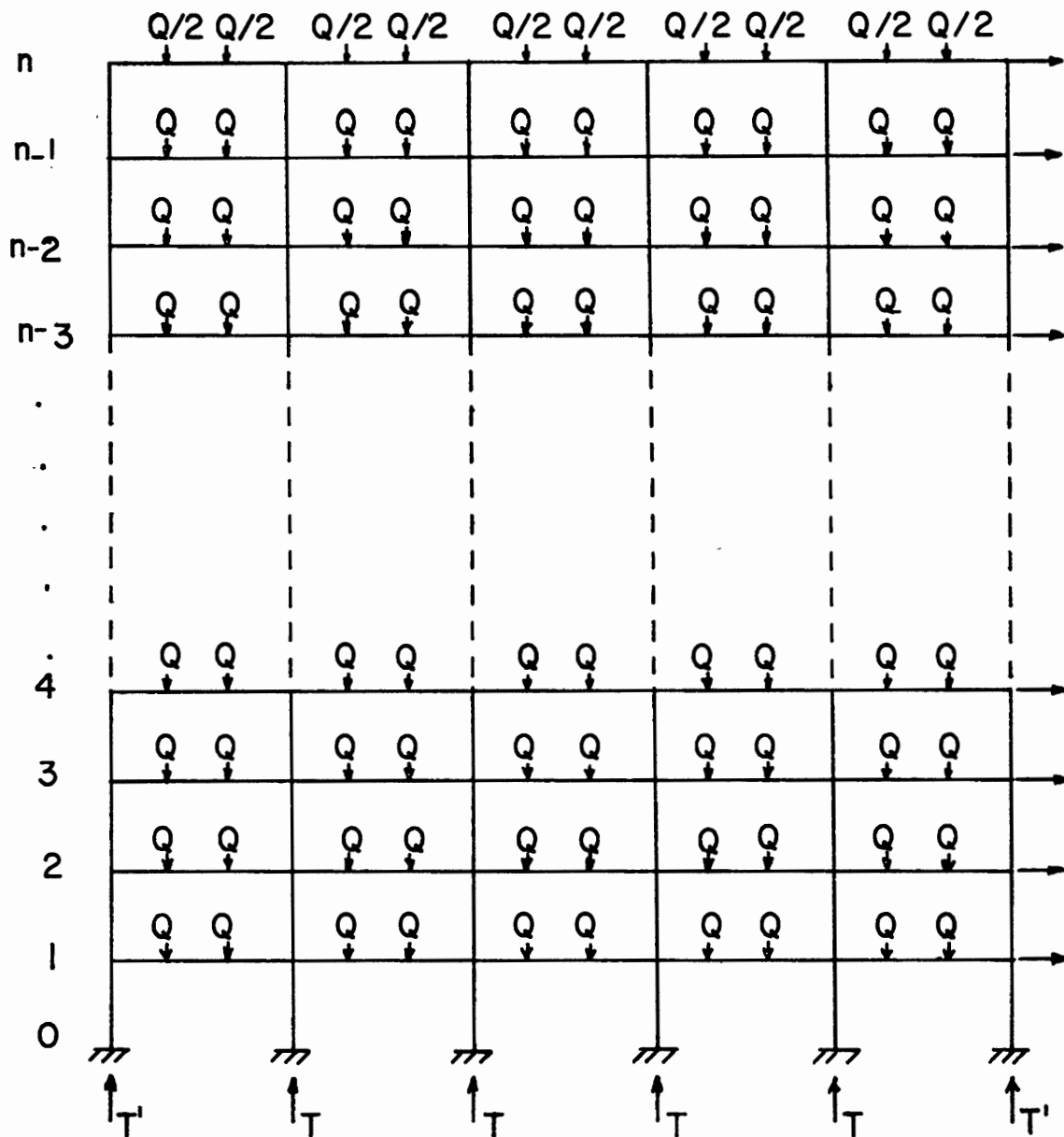
In this chapter, overall loading patterns, load relationships with some simplifying assumptions, different types of frame failure, and some general requirements of structural similitude will be discussed. The purpose of this chapter is to set the background stage for the analytical treatment which follows in Chapters III and IV.

2.2 THE MODEL OF UNBRACED FRAME

In designing a reinforced concrete building frame, several loading patterns must be considered. A critical condition for frame instability exists when all floors are fully loaded, thus creating full axial loads in columns. An unbraced n-story concrete frame is shown in Fig. 2.1. The width of each bay (beam length) and the story to story height (column length) are L_b and L_c respectively. It is assumed that the center to center distance between frames is also equal to L_b .

A two bay interior panel which represents a typical interior panel is shown in Fig. 2.2. Due to symmetry of the frame points of inflection are at column midheights and for simplicity a reduced model as shown in Fig. 2.3 will be analyzed. According to Rad (12) for a single panel the relationship between column load P (applied at top) and beam load Q , neglecting the increased column load due to lateral load, can be expressed as:

$$Q/P = 1/(2n-2) \quad (2.1)$$



- Q - beam loads, applied at third points
- $Q/2$ - roof loads, applied at third points
- L_b - width of the bay
- L_c - story to story height
- T - interior column thrust

Figure 2.1. A multi-story unbraced concrete frame

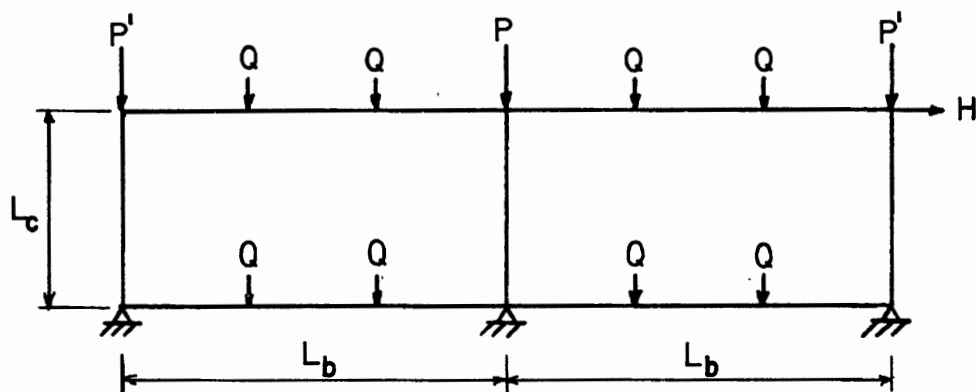


Figure 2.2. An interior panel

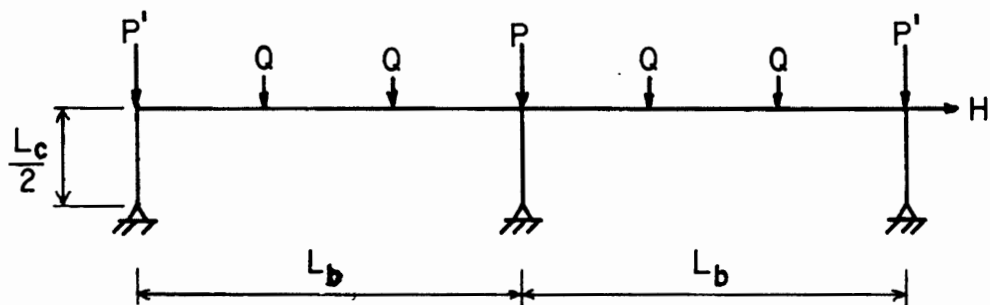


Figure 2.3. The reduced model frame

And the relationship between the column thrust T and the beam load Q as:

$$Q/T = 1/(2n-1) \quad (2.2)$$

where n = number of stories. Considering the reduced model shown in Fig. 2.3, equation 2.1 is not valid for 2-bay frame, however, it will be shown later that Equation 2.2 is still true. For a 2-bay frame, the applied column loads P and P' must be chosen such that the column thrusts T are all the same. For the exterior and interior column loads P' and P at the first floor, the corresponding equations become:

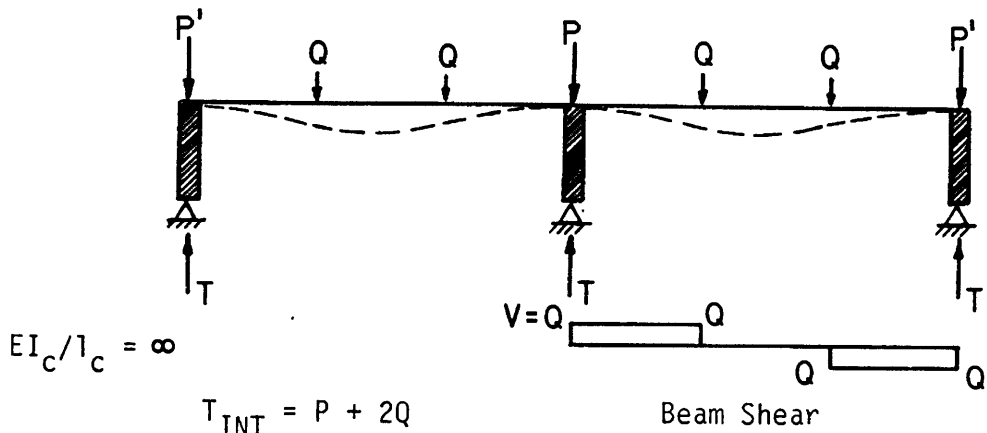
$$Q/P' = 1/(2n-2); \text{ and} \quad (2.3)$$

$$Q/P = 1/(2n-3) \quad (2.4)$$

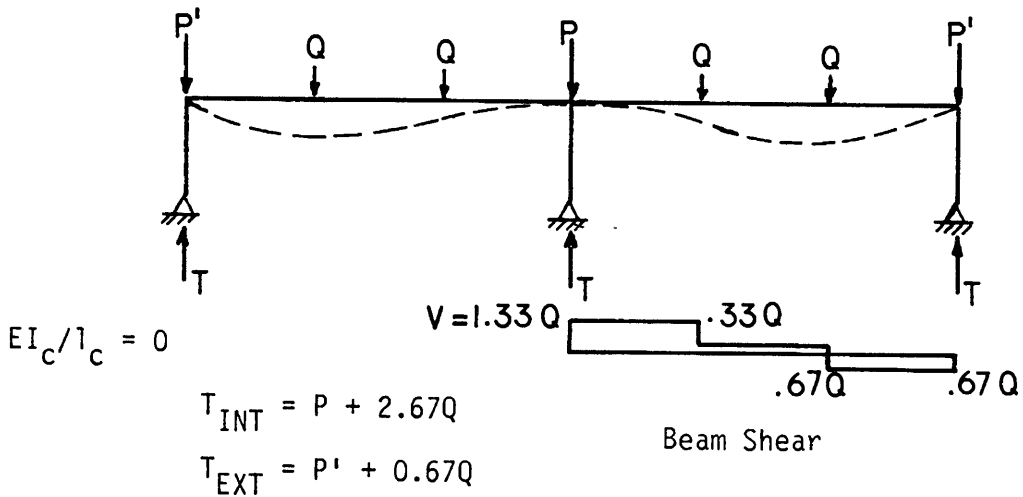
Equation 2.2 will remain unchanged. Again, for Equation 2.3 and 2.4 the increased column load caused by the lateral load H is neglected. Now let us examine these relationships for two extreme conditions condition I for "very stiff" columns, and condition II for "very slim" columns, as shown in Fig. 2.4.

The beam shear distribution varies as relative column/beam stiffness ratio changes, thus influencing the interior and exterior column thrusts. However, this variation is small. As an example, the extreme boundaries of column thrust values are shown for $n = 5$, in Fig. 2.5. As n increases, the range of variation decreases.

For simplicity of analytical treatment, the beam shear distribution and thus the column thrusts of Condition I are assumed to exist in all frames, regardless of column/beam stiffness ratio. So the interior column thrust will be assumed as the interior column load plus $2Q$; and

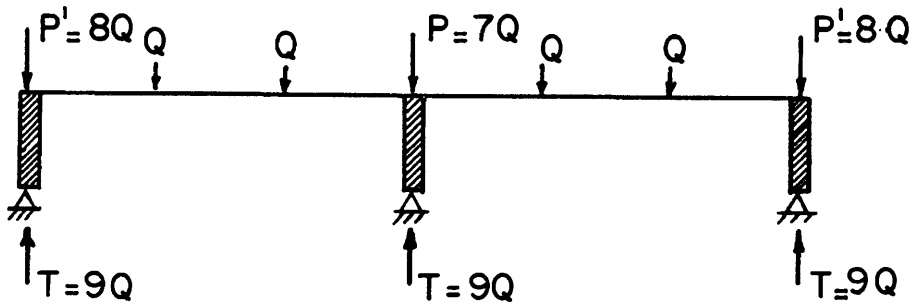


(a) Extreme condition I, very stiff columns

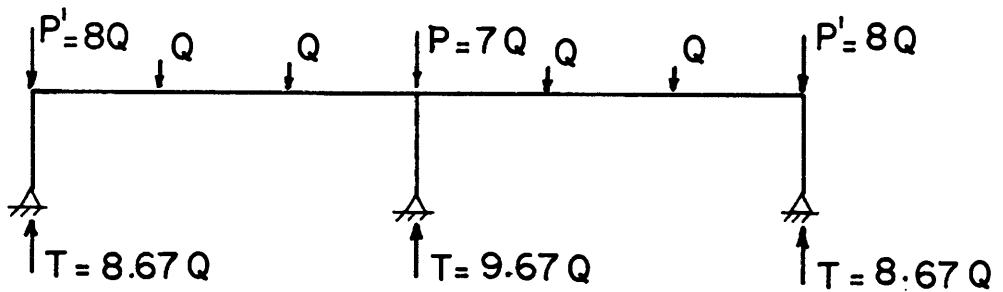


(b) Extreme condition II, very slim columns

Figure 2.4. Two extreme conditions



(2.5a) Extreme condition I: very stiff columns



(2.5b) Extreme condition II: very slim columns

Figure 2.5. Example of a 5-story building at two extreme conditions

the exterior column thrust as the exterior column load plus Q .

2.3 DESCRIPTION OF THE TYPES OF FRAME FAILURE

The primary purpose of this research is to study the behavior of a two-bay unbraced reinforced concrete frame under the influence of gravity and lateral loads.

Based on the ACI-77 Code (4), Article 9.2.2, if resistance to structural effects of lateral load is included in design, 75% of factored gravity and lateral load must be considered. Accordingly, the behavior of the frame acted on by 75% of factored gravity and lateral loads will be studied.

The frame loading sequence will be:

1. apply the gravity loads up to 75% of their design value,
2. then apply the lateral load H until frame failure occurs.

According to Rad (12), there are four types of failure which can occur in the frame.

1. Type I - Elastic Frame Instability

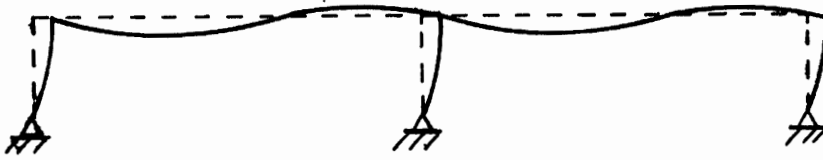
This frame, as shown in Fig. 2.6 (a) becomes unstable under large column loads. The failure is analogous to elastic column or frame buckling.

2. Type II - Material Failure

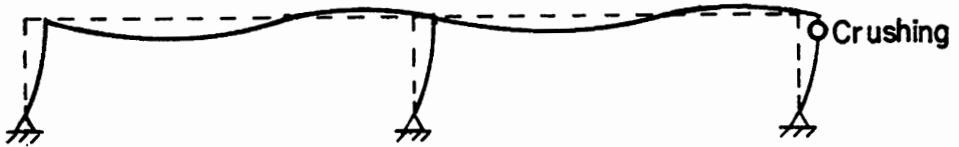
This failure exists when any section of a column fails by crushing of the concrete. (Fig. 2.6 (b))

3. Type III - Frame Instability with Partial Plasticity

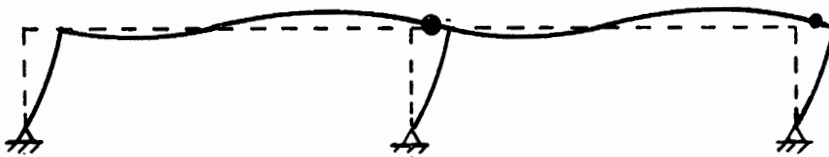
After the lateral load H is applied, the frame remains in stable condition until two plastic hinges form at critical sections of the frame. The lateral load which causes the



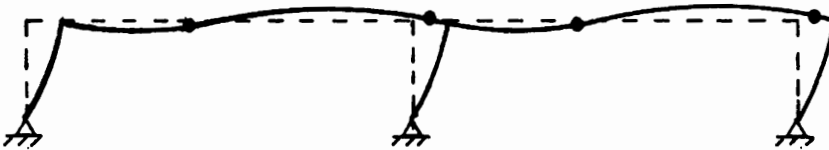
(a) Type I, elastic frame instability.



(b) Type II, material failure



(c) Type III, frame instability with partial plasticity



(d) Type IV, frame instability with panel mechanism

Figure 2.6. Types of frame failure

first set of plastic hinge to form is designated by H_1 . In this type of failure, due to the loss of frame stiffness after the first hinges, the frame can no longer stay in stable equilibrium position. (Fig. 2.6 (c))

4. Type IV - Frame Instability with Development of a Panel Mechanism

The frame will stay in a stable equilibrium until enough plastic hinges form in the frame to produce an unstable mechanism. The extra lateral load beyond H_1 that is necessary to produce a mechanism is designated by H_2 . (Fig. 2.6 (d))

In this present study, we will not focus on Types I and II failure, but the boundary between Types III and IV failure will be examined.

The lateral load terminology will be as follows:

$$H = H_1 + H_2$$

where: H = Total lateral load which is resisted by the frame

H_1 = Lateral load to produce the first set of two plastic hinges

H_2 = Lateral load in excess of H_1 to produce the panel mechanism

Also, a useful index can be introduced as the percentage of moment redistribution, defined as β ,

$$\beta = (H_2/H)(100) \tag{2.5}$$

for Type III failure:

$$H_2 = 0, \quad \beta = 0, \quad \text{and} \quad H = H_1$$

for Type IV failure:

$$H_2 > 0, \quad \beta > 0, \quad \text{and} \quad H = H_1 + H_2$$

2.4 LOADING OF THE PROTOTYPE VS. MODEL FRAMES

In this section an interior bay of a multistory structure will be considered (Fig. 2.7) and the loading relationship between the prototype and the model with regard to scale factor (SF), structural analysis, and member strength will be determined.

2.4.1 Frame Loading. Considering Fig. 2.8, one may write:

$$\text{Total beam load} = (\omega \ell)L_b = 2Q, \text{ and}$$

$$\text{Column thrust, } T = (\omega \ell)L_b \text{ for each floor}$$

where: ω = uniform load per unit area

ℓ = bent spacing

As discussed before:

$$Q/T = 1/2n-1 \quad (2.2)$$

$$\text{or} \quad 2Q/2T = 1/2n-1$$

$$\text{or} \quad (\omega \ell)L_b/2T = 1/2n-1 \quad (2.6)$$

Equation 2.6 establishes the relationship between column thrust T and number of stories n for a uniform surface load ω .

2.4.2 Column Strength. In this section, the relation between the column axial capacities of the model and the prototype is determined.

$$P_{no} = \text{pure axial load capacity} = 0.85 f'_c A_c + (\rho A_g) f_y$$

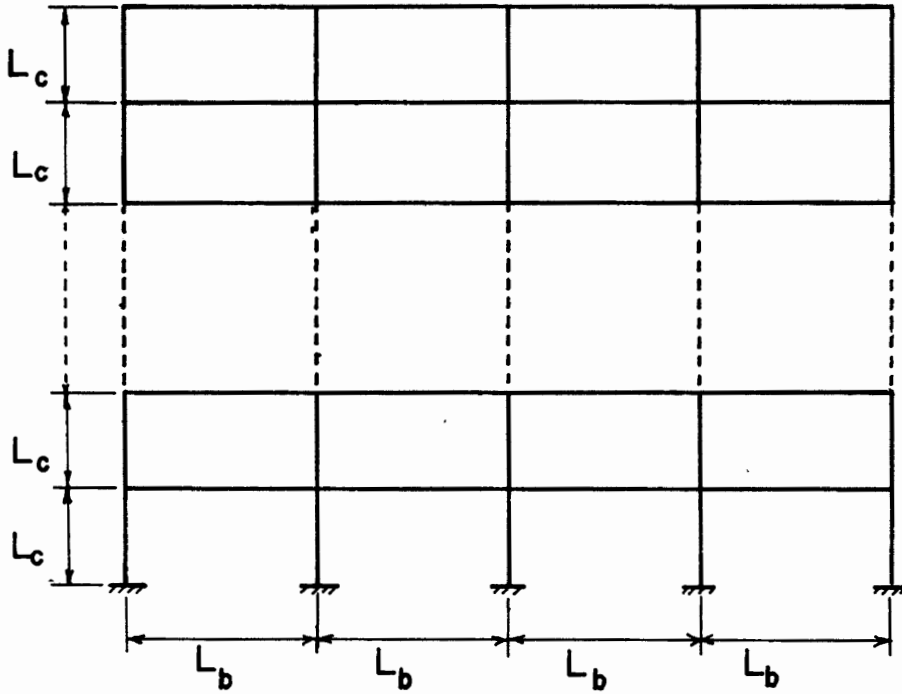


Figure 2.7. A multi-story frame

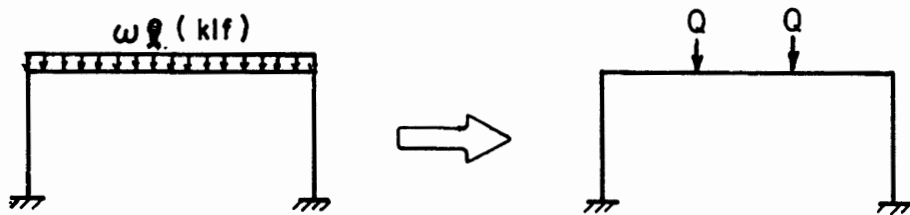


Figure 2.8. An interior bay

$$\frac{P_{no(m)}}{P_{no(p)}} = \frac{0.85 f'_c (A_{g_m} - \rho_m A_{g_m}) + (\rho_m A_{g_m}) f_y}{0.85 f'_c (A_{g_m} - \rho_p A_{g_p}) + (\rho_p A_{g_p}) f_y} \quad (2.7)$$

where "m" and "p" refer to model and prototype respectively. The comparison of the section properties between prototype and the model is summarized in Table 2.1.

By substituting for A_{g_p} in terms of A_{g_m} in Equation 2.7, the following is obtained:

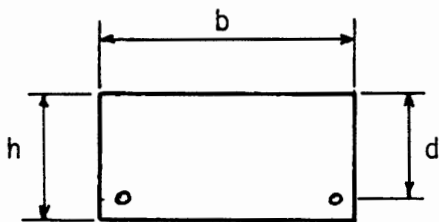
$$\frac{P_{no(m)}}{P_{no(p)}} = \frac{A_{g_m} [0.85 f'_c (1-\rho) + \rho f_y]}{(1/SF)^2 A_{g_m} [0.85 f'_c (1-\rho) + \rho f_y]}$$

$$\text{or } P_{no(p)} = (1/SF)^2 (P_{no(m)}) \quad (2.8)$$

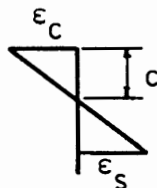
For example, for a scale factor of 1/3, we get:

$$P_{no(p)} = 9P_{no(m)}$$

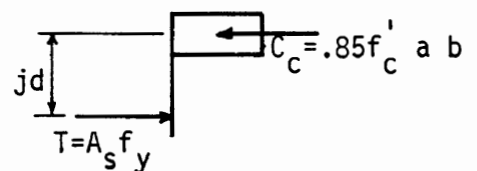
2.4.3 Beam Strength. In this section, the relationship between the beam moment capacity of the model and prototype is determined.



beam cross section



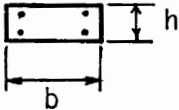
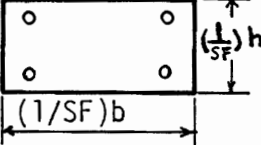
strain diag



rectangular stress block

TABLE 2.1

COMPARISON OF SECTION PROPERTIES FOR
THE MODEL AND THE PROTOTYPE

Model	Prototype
 <p> f'_c f_y $\rho_m = \rho$ A_{g_m} </p>	 <p> f'_c f_y $\rho_p = \rho$ $A_{g_p} = (1/SF)^2 A_{g_m}$ </p>

SF = scale factor = model dimension/
prototype dimension

if $M = A_s f_y (jd)$, and $\rho = A_s/bd$

$$M_m = A_{s_m} f_y j d_m$$

and $M_p = A_{s_p} f_y j d_p$

$$M_p/M_m = A_{s_p} f_y j d_p / A_{s_m} f_y j d_m$$

$$\text{or } \frac{M_p}{M_m} = \frac{[\rho (1/SF * b_m)(1/SF * d_m)] f_y (j) (1/SF * d_m)}{[\rho (b_m)(d_m)] f_y (j) (d_m)}$$

$$\text{or } M_p = (1/SF)^3 (M_m) \quad (2.9)$$

For example, for a scale factor of 1/3, we get:

$$M_p = 27 (M_m)$$

2.4.4 The Structural Analysis. In this section, the structural analysis with regard to the column axial thrust and beam moment will be considered. Let us consider column load first.

$$P_p = (\omega_p \ell_p) L_{b_p} \quad \text{and} \quad P_m = (\omega_m \ell_m) L_{b_m}$$

$$P_p/P_m = (\omega_p \ell_p) L_{b_p} / (\omega_m \ell_m) L_{b_m}$$

$$\text{or } \frac{P_p}{P_m} = (\omega_p/\omega_m) \left[\frac{(1/SF)^2 \ell_m L_{b_m}}{\ell_m L_{b_m}} \right]$$

$$\text{or } P_p/P_m = (1/SF)^2 (\omega_p/\omega_m) \quad (2.10)$$

For example, for a scale factor of 1/3, we get:

$$P_p/P_m = (9) (\omega_p/\omega_m)$$

Now considered are the beam moments, which are caused by the beam load (ωl) , and are functions of $(\omega l)(L_b^2)$. The moment coefficients which define the moments at various beam locations may be obtained from the ACI code 318-77 (4).

$$M_p = k(\omega_p l_p L_{b_p}^2)$$

$$\text{and } M_m = k(\omega_m l_m L_{b_m}^2)$$

where k is moment coefficient

$$\frac{M_p}{M_m} = \frac{k(\omega_p l_p L_{b_p}^2)}{k(\omega_m l_m L_{b_m}^2)} = \frac{\omega_p l_p L_{b_p}^2}{\omega_m l_m L_{b_m}^2}$$

$$\frac{M_p}{M_m} = (\omega_p/\omega_m) \left[\frac{(1/SF)^3 l_m L_{b_m}^2}{l_m L_{b_m}^2} \right]$$

$$\text{or } M_p/M_m = (1/SF)^3 (\omega_p/\omega_m) \quad (2.11)$$

For example, for a scale factor of 1/3, we get:

$$M_p/M_m = (27)\omega_p/\omega_m$$

Now by setting Equation 2.8 equal to Equation 2.10 we obtain:

$$P_p/P_m = (1/SF)^2 = (1/SF)^2 (\omega_p/\omega_m)$$

$$\therefore \omega_p = \omega_m$$

Also by setting Equation 2.9 equal to Equation 2.11 we obtain:

$$M_p/M_m = (1/SF)^3 = (1/SF)^3 (\omega_p/\omega_m)$$

$$\therefore \omega_p = \omega_m$$

In summary, we conclude that:

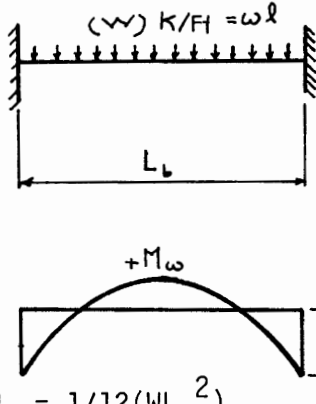
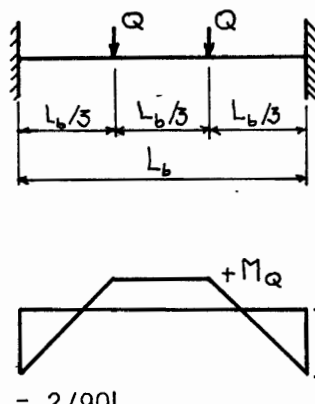
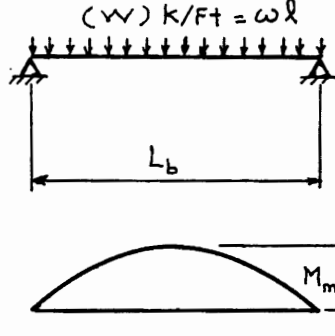
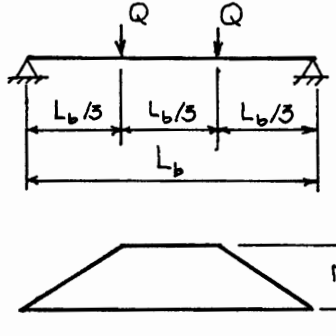
$$\omega_p = \omega_m \tag{2.12}$$

The above equation indicates that the surface loading (psf) of the prototype and the model frame are equal and independent of the scale factor (SF). Since testing a frame by a couple of concentrated loads is much easier than by uniform load, a relationship is found between the concentrated load Q and the uniform load of ωl . Table 2.2 summarizes the related equations.

In conclusion, it may be stated that if two concentrated loads $Q = 3/8 (\omega l)L_b$ are applied at beam third points, the moment effects will be the same as uniform load (ωl). Therefore, for either analytical or physical testing of the frame, two concentrated loads each equal to $Q = 3/8 \omega l L_b$, must be applied at beam third points in order to simulate uniform load ωl moments.

In all analytical modeling in this investigation, concentrated loads at beam third points were applied.

THE RELATION BETWEEN UNIFORM AND CONCENTRATED LOADS

Uniform Loading System	Concentrated Loading System
 <p> $(w) \text{ k/ft} = w l$ L_b $+M_w$ $-M_w$ $-M_w = 1/12 (w L_b^2)$ $+M_w = 1/24 (w L_b^2)$ </p>	 <p> Q Q $L_b/3$ $L_b/3$ $L_b/3$ L_b $+M_Q$ $-M_Q$ $-M_Q = 2/9 Q L_b$ $+M_Q = 1/9 Q L_b$ </p>
<p>NEGATIVE MOMENT SET $M_w = M_Q$ $1/12 (w L_b^2) = 2/9 (Q L_b)$ $\therefore Q = 3/8 (w L_b)$ </p>	<p>POSITIVE MOMENT SET $M_w = M_Q$ $1/24 (w L_b^2) = 1/9 (Q L_b)$ $\therefore Q = 3/8 (w L_b)$ </p>
 <p> $(w) \text{ k/ft} = w l$ L_b $M_{max} = M_w$ $M_w = 1/8 (w L_b^2)$ </p>	 <p> Q Q $L_b/3$ $L_b/3$ $L_b/3$ L_b M_Q $M_Q = 1/3 (Q L_b)$ </p>
<p>SET $M_w = M_Q$ $1/8 (w L_b^2) = 1/3 (Q L_b)$ $\therefore Q = 3/8 (w L_b)$ </p>	
<p>SUMMARY: from the above two results, we conclude: $Q = 0.375 (w l) L_b = 0.375 (w L_b)$ </p>	

$W(k/ft) = [w(k/ft^2)] * l = (w l) k/ft$

CHAPTER III

ELASTO-PLASTIC MODEL

3.1 GENERAL

The stability of unbraced frames using an analytical method will be discussed in this chapter. This method consists of the mathematical solution of an elasto-plastic stability model. This solution will define the boundaries where limit design may be feasible.

In this stability analysis, the reduced model of Fig. 3.1 is investigated. The behavior of the model frame as acted upon by column loads, beam loads, and lateral force is studied. The stability equation of the frame, when frame becomes unstable is determined by the principle of neutral equilibrium. The stability equation is also determined by Bolton's (15) method.

The stability equation of the frame when it becomes unstable under the action of gravity loads alone without lateral load is also determined.

3.2 FRAME LOADING, ASSUMPTIONS, AND NOTATION

The loading sequence for this model frame is in accordance with ACI 318-77, Art. 9.2.2, as discussed in Sec. 2.3. Axial column loads P and beam loads Q are first applied proportionally up to 75% of the predicted ultimate capacity of the frame. Next, lateral load H is applied until total failure of the frame is reached. The lateral deflection of the model is half that of the actual frame.

In the stability analysis of the model, the following assumptions (12) are made:

1. The beam members and column members possess an elasto-plastic

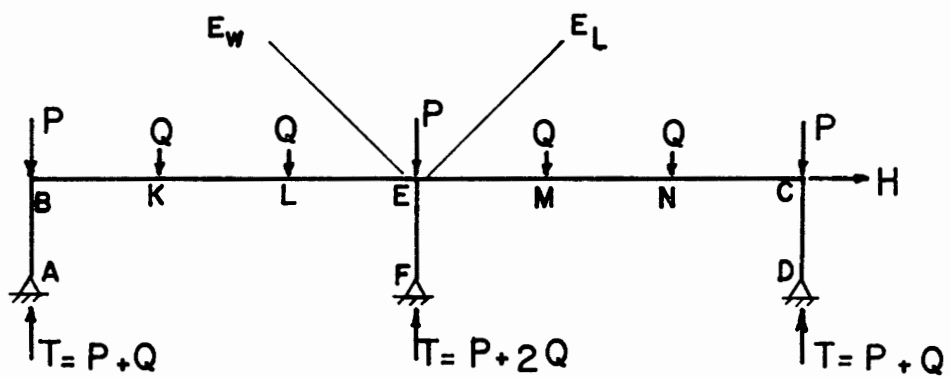


Figure 3.1. The reduced model frame

moment-curvature ($M-\phi$) relationship. Also, the flexural rigidities of the column (EI_c) and the beam (EI_b) do not vary along the length of the members.

2. The change in the magnitude of column thrust caused by the lateral force H , is neglected.
3. The change in moment due to the product of column axial thrust and the column deflection from the chord connecting the column ends is neglected, i.e., the moment diagram is triangular.
4. The beam bending moment capacity, M_p , for the negative and positive bending is the same.

The reduced model frame of Fig. 2.3 is used for analysis with the difference that, for simplicity, all column axial loads are assumed to be equal to P as shown in Fig. 3.1. This frame is examined at two stages of loading:

1. The first stage exists until the first hinges are developed at corner C and section E_w due to gravity loads P , Q , and the horizontal load H_1 .
2. The second stage exists after plastic hinges form at point k and M due to the additional horizontal force H_2 .

The definitions of symbols used in the following discussion are given below:

- | | |
|-------|---|
| P | axial load on the column |
| Q | applied load on the beam third points |
| L_b | length of the beam |
| L_c | length of the column |
| M_p | plastic moment capacity of the beam (or column) |

EI_b flexural stiffness of the beam

EI_c flexural stiffness of the column

ψ relative flexural stiffness of the column and beam

$$= \frac{EI_c/L_c}{EI_b/L_b}$$

H lateral load applied at corner C

H_1 lateral load required for the formation of the first hinges in the frame (at corner C and E_w)

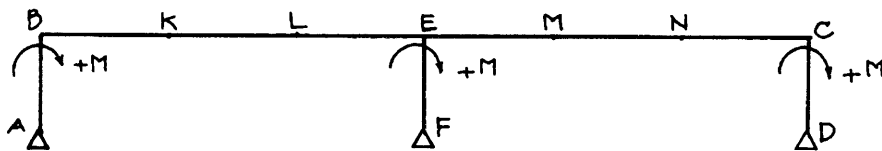
H_2 additional lateral load required for the formation of the second hinges in the frame (at k and M)

Δ horizontal deflection of the frame

Δ_1 horizontal deflection of the frame at the formation of first hinges

Δ_2 additional horizontal deflection of the frame at the formation of second hinges.

Sign Convention: Clockwise moment on the columns at corners B, E and C is positive



All moment diagrams are drawn on the compression side of the members. The gravity moments at corners B, E and C are determined by the method of moment distribution. Since the column base is hinged and the beam is bent symmetrically, the determination of distribution factor (DF) for the column is as follows:

For column AB and CD:

$$DF = \frac{3/4 [EI_c/L_c/2]}{3/4 [EI_c/L_c/2] + 1/2 [EI_b/L_b]}$$

After substitution of ψ , the above equation will simplify to:

$$DF = 3\psi/(3\psi + 1)$$

For column EF:

$$DF = \frac{3/4 [EI_c/L_c/2]}{3/4 [EI_c/L_c/2] + 2(0.5 EI_b/L_b)}$$

which after substitution of ψ , will simplify to:

$$DF = 3\psi/(3\psi + 2)$$

The DF is multiplied by the fixed end moment caused by the beam load Q.

Therefore the moment is:

$$M = (3\psi/(3\psi + 1)) * (2/9 Q L_b)$$

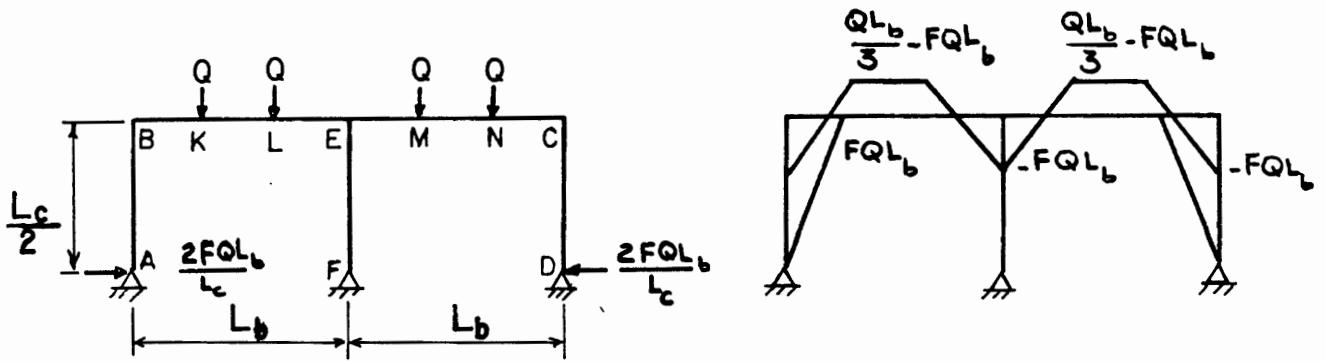
$$\text{or } M = (6\psi/27\psi + 9)Q L_b = (2\psi/(9\psi + 3)) Q L_b$$

denoting $2\psi/(9\psi + 3)$ by F:

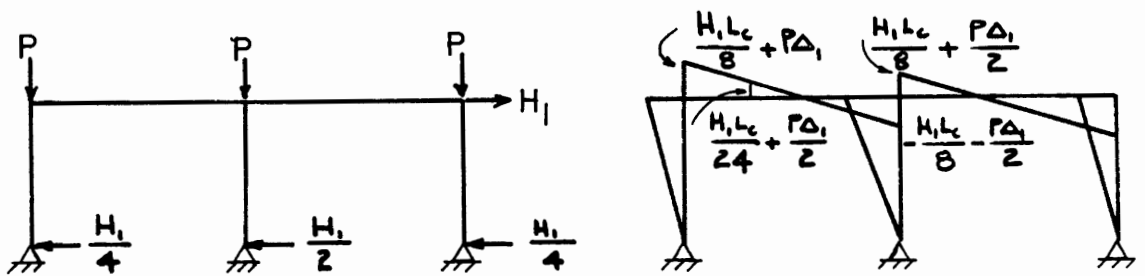
$$M = F Q L_b$$

3.3 CONDITION OF THE FRAME AT THE FIRST HINGE

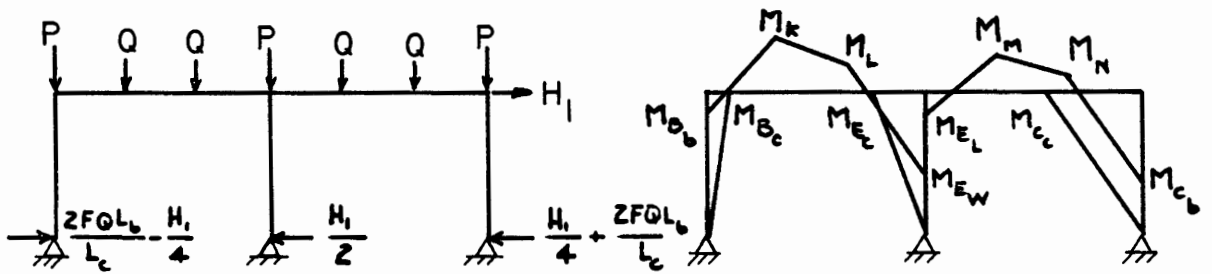
The loads and the corresponding moment diagrams until the first hinges form at E_w and C are shown in Fig. 3.2. For simplicity of calculations, moments are divided into two parts. Part one is the moments due to beam loads Q, as shown in Fig. 3.2a. Part two is the moments due to column axial thrust P, horizontal lateral load H_1 , and the lateral deflection Δ_1 , as shown in Fig. 3.2b.



(a) Beam loads Q and moments



(b) Lateral load H_1 , column loads P , and moments



(c) Total loads and moments

Figure 3.2. Loads and moments at the first hinge

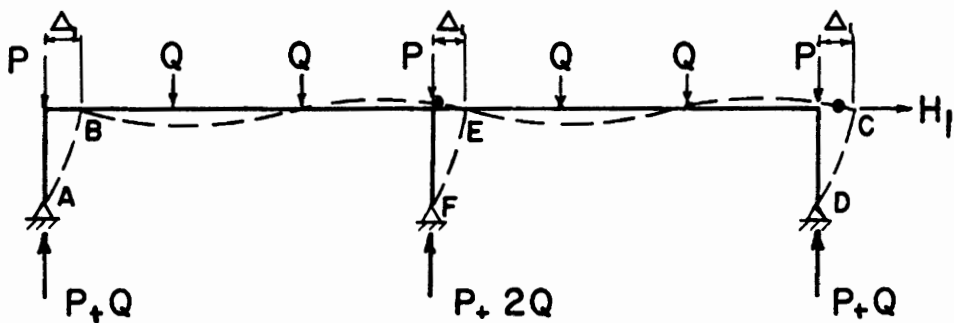


Figure 3.3. Loads and deflected shape at the first hinge

At the formation of first plastic hinges the moment capacity of the beam (or column) is reached at corners E_w and C. Therefore:

$$\begin{aligned} & -F Q L_b - H_1 L_c / 8 - (P + Q) \Delta_1 = -M_p \\ \text{or} \quad & M_p - F Q L_b = H_1 L_c / 8 + (P + Q) \Delta_1 \end{aligned} \quad 3.1$$

Total moments, according to Fig. 3.2c are:

$$\begin{aligned} M_{B_b} &= -F Q L_b + H_1 L_c / 8 + (P + Q) \Delta_1 \\ M_{B_c} &= F Q L_b - H_1 L_c / 8 - (P + Q) \Delta_1 \\ M_K &= Q L_b / 3 - F Q L_b + H_1 L_c / 24 + (P+Q)\Delta_1 / 2 \\ M_L &= Q L_b / 3 - F Q L_b - H_1 L_c / 24 \\ M_{E_w} &= -F Q L_b - H_1 L_c / 8 - (P+Q)\Delta_1 / 2 \\ M_{E_c} &= -H_1 L_c / 4 - (P + Q)\Delta_1 \\ M_{E_L} &= -F Q L_b + H_1 L_c / 8 + (P+Q)\Delta_1 / 2 \\ M_M &= Q L_b / 3 - F Q L_b + H_1 L_c / 24 \\ M_{C_b} &= -F Q L_b - H_1 L_c / 8 - (P + Q)\Delta_1 \\ M_{C_c} &= -F Q L_b - H_1 L_c / 8 - (P + Q)\Delta_1 \end{aligned}$$

Fig. 3.3 shows loads and frames deflected shape at the first hinge.

3.4 CONDITION OF THE FRAME AFTER THE FIRST HINGES

After the first hinges form, additional moment is caused by lateral load H_2 and additional deflection Δ_2 . First let us determine how the lateral load H_2 and the moment caused by deflection Δ_2 are going to be distributed throughout the frame.

3.4.1 Shear Distribution by Using a Spring Model. Let us consider the (Δ_2) effect only which is caused by lateral force H_2 . Since moment at joint C has reached its capacity M_p , the model can be reduced to what is shown in Fig. 3.4. This reduced model can be further simplified to a set of springs having a stiffness of k . As the tensile force H_2 is applied, both springs will be stretched the same amount of Δ_2 . The tensile force in each spring will be equal to $H_2/2$. Therefore by this reasoning the horizontal shear distribution at the column supports of A and F due to lateral force H_2 will be equal to $H_2/2$.

As the frame deflects, the moment at corner E_w and C must remain constant at moment capacity, M_p . Therefore the added moment, $(P+Q)\Delta_2$, on the column CD must be opposed by a horizontal shear force equal to $2(P+Q)\Delta_2/L_c$. This shear force is transferred to column EF and AB such as to keep the frame in equilibrium.

Again by considering the spring model shown in Fig. 3.4 and the analogy explained above, this shear force must be distributed equally at the column supports A and F, as shown in Fig. 3.5a.

By combining the $P-\Delta_2$ and the lateral load H_2 effects, the shear distribution as shown in Fig. 3.5b is obtained.

3.4.2 Shear Distribution by Yura's Method. A second technique presented by Yura (13) may be used to determine the horizontal shear distribution at the supports of A, F and D.

In general, the total gravity load which produces sidesway can be distributed among the columns in a story in any manner. Sidesway will not occur until the total frame load on a story reaches the sum of the potential individual column loads for the unbraced frame. In our model

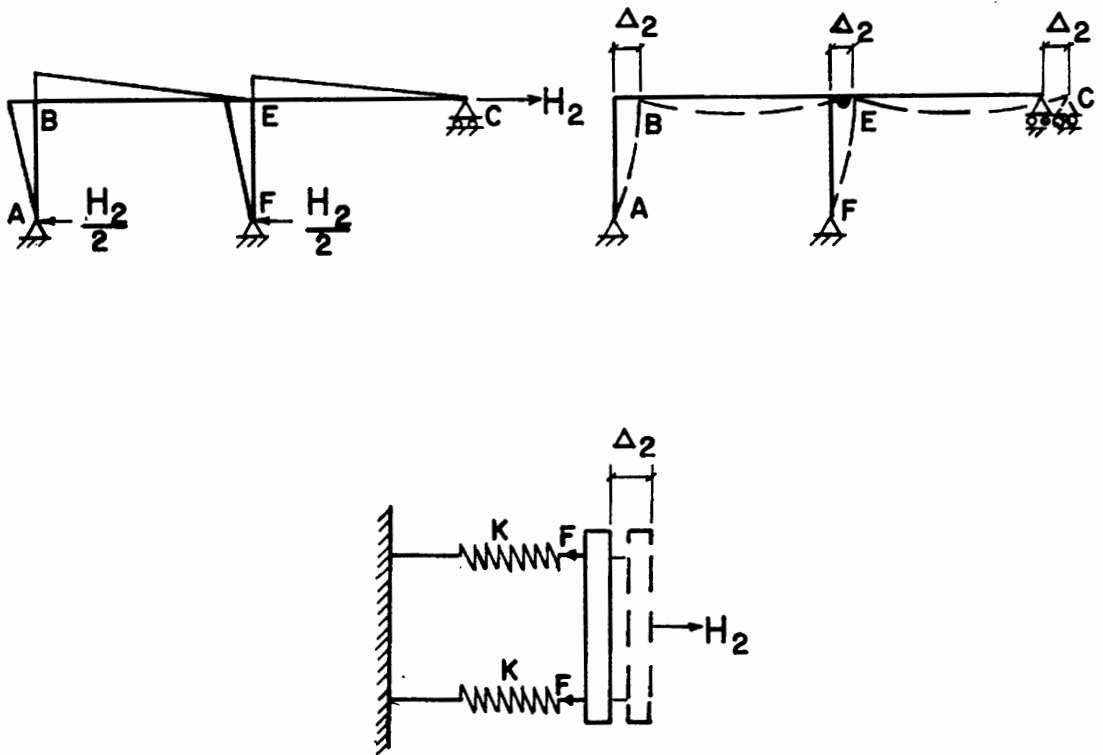
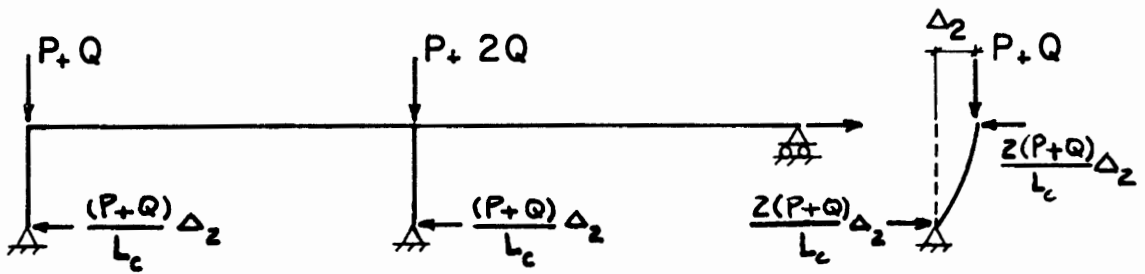
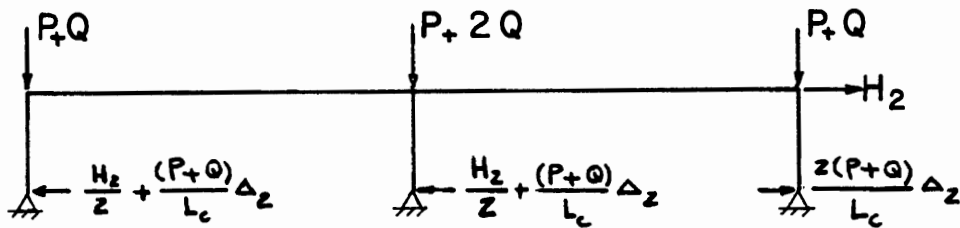


Figure 3.4. Spring model and the shear distribution caused by lateral load



(a) Shear distribution due to P- Δ effect only



(b) Total shear distribution after the first hinge

Figure 3.5. Shear distribution by using a spring model

frame the total frame load is $(3P + 4Q)$.

After the first hinges occur, since column CD is then "hinged-hinged" it is no longer stable. Thereafter the frame loads must be carried by the two remaining healthy columns AB and EF. In addition to its own load, each column must support an additional P- Δ moment equal to $(P+Q)\Delta_2/2 = 0.5 (P+Q)\Delta_2$ which is caused by the deflection of column CD. This is equivalent to an additional axial load equal to $0.5(P+Q)$ on the healthy columns. Consequently column AB must be able to support a fictitious axial load of $(P+Q) + 0.5(P+Q) = 1.5(P+Q)$, and column EF, a load of $(P+2Q) + 0.5(P+Q) = 1.5(P+Q) + Q$. Considering column AB and EF as shown in Fig. 3.6a:

$$M_{(P\Delta)} = 1.5(P+Q)\Delta_2 = (P+Q)\Delta_2 + V_1 (L_c/2)$$

from which: $V_1 = (P+Q)\Delta_2/L_c$

$$M_{(P\Delta)} = [1.5(P+Q) + Q] \Delta_2 = (P+2Q)\Delta_2 + V_2 (L_c/2)$$

from which: $V_2 = (P+Q)\Delta_2/L_c$

By the spring model of Fig. 3.4, the horizontal shear distribution at supports A and F caused by lateral load H_2 are each equal to $H_2/2$.

By superposition of P- Δ and lateral load effects, one can conclude the shear distribution as shown in Fig. 3.6b which is identical to what was found by the spring model. Loads and the corresponding moments after the first hinge, along with the shear distribution are shown in Fig. 3.7.

3.5 CONDITION OF THE FRAME WHEN THE SECOND HINGES FORM AT (K) and (M)

The total moment at (K) and (M) must include those caused by gravity loads P and Q, those due to lateral loads H_1 and H_2 , and their corresponding deflections Δ_1 and Δ_2 . Let us consider joint K.

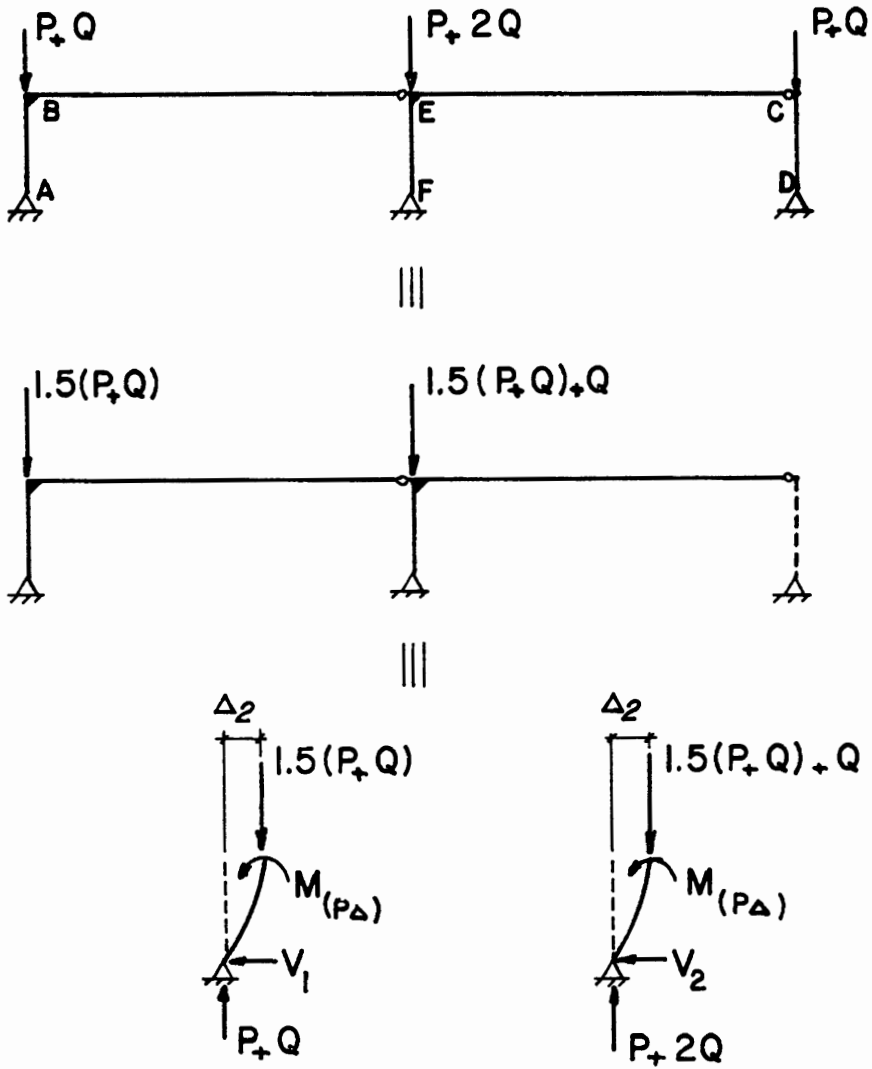
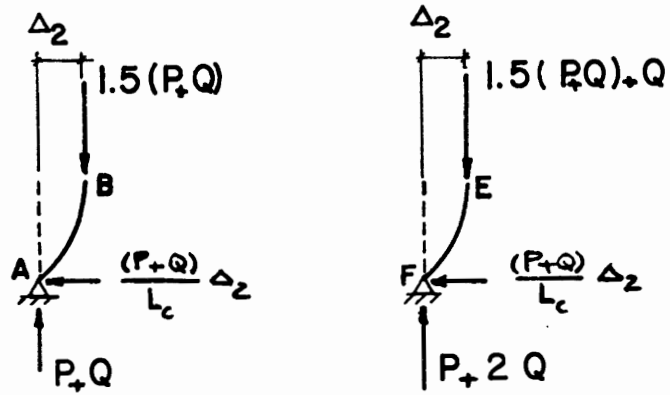


Figure 3.6a Horizontal shear distribution after the first hinges due to $P-\Delta$ effect only



Due to P- Δ effect only

+



Due to lateral and H_2 , only

III

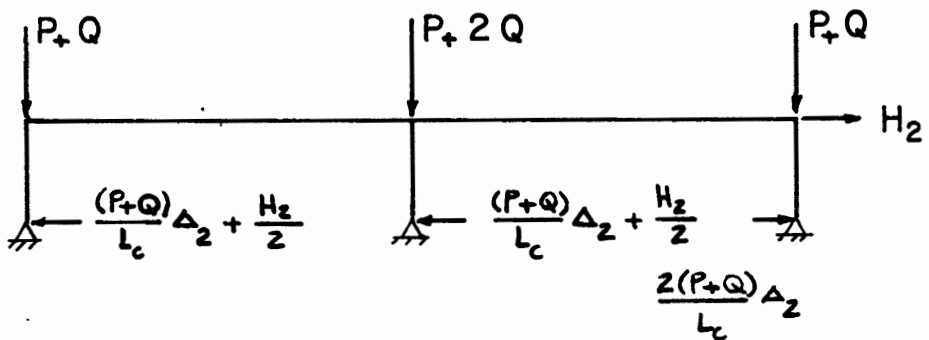
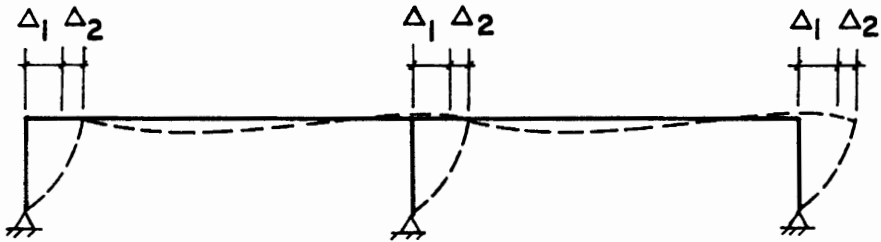
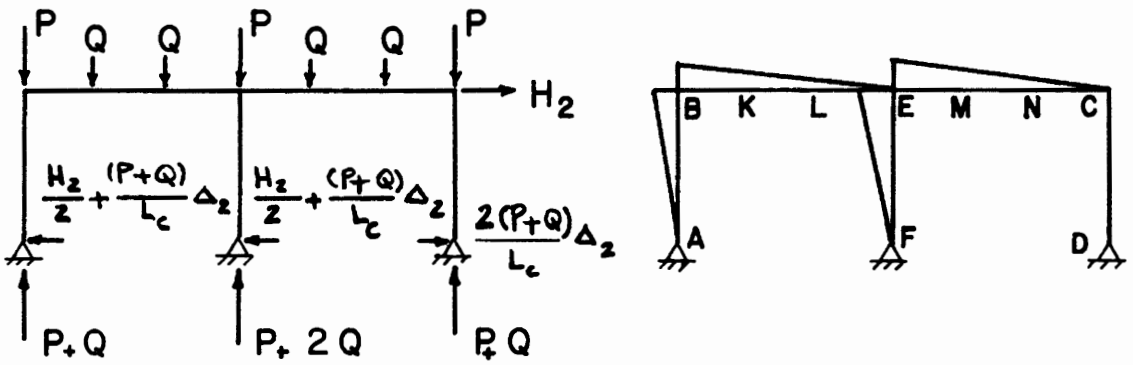


Figure 3.6b. Gravity and the lateral loads, and the horizontal shear distribution after the first hinge



$$M_{B_c} = -\frac{H_2 L_c}{4} - \frac{3}{2} (P+Q) \Delta_2$$

$$M_{B_b} = \frac{H_2 L_c}{4} + \frac{3}{2} (P+Q) \Delta_2$$

$$M_K = \frac{H_2 L_c}{6} + (P+Q) \Delta_2$$

$$M_L = \frac{H_2 L_c}{12} + \frac{(P+Q)}{2} \Delta_2$$

$$M_{E_c} = -\frac{H_2 L_c}{4} - \frac{(3P+5Q)}{2} \Delta_2$$

$$M_{E_L} = \frac{H_2 L_c}{4} + \frac{(3P+5Q)}{2} \Delta_2$$

$$M_M = \frac{H_2 L_c}{6} + \frac{(3P+5Q)}{3} \Delta_2$$

$$M_N = \frac{H_2 L_c}{12} + \frac{(3P+5Q)}{6} \Delta_2$$

Figure 3.7. Loads, moments, and the deflected shape caused by the additional lateral load H_2 and deflection Δ_2

The moment caused by gravity loads P and Q, lateral load H_1 and its respective deflection Δ_1 , is:

$$M_K = Q L_b/3 - F Q L_b + H_1 L_c/24 + (P+Q)\Delta_1/2 \quad 3.2$$

The moment caused by lateral load H_2 and its respective deflection Δ_2 , is:

$$M_K = H_2 L_c/6 + (P+Q)\Delta_2 \quad 3.3$$

Therefore the total moment at K is found by addition of equations 3.2 and 3.3. Since at collapse this total is equal to M_p :

$$M_p = \left[Q L_b/3 - F Q L_b + H_1 L_c/24 + (P+Q)\Delta_1/2 \right. \\ \left. [H_2 L_c/6 + (P+Q)\Delta_2] \right]$$

which after simplifying and rearranging gives:

$$H_2 L_c/2 = 3M_p - Q L_b + 3F Q L_b + \left[-H_1 L_c/8 - (P+Q)\Delta_1 \right] - \\ \left[(P+Q)\Delta_1/2 \right] - 3(P+Q)\Delta_2 \quad 3.4$$

Now substitute for the value of $\left[H_1 L_c/8 + (P+Q)\Delta_1 \right]$ and $\left[(P+Q)\Delta_1/2 \right]$ from equation 3.1 into equation 3.4:

$$H_2 L_c/2 = 3M_p - Q L_b + 3 F Q L_b - M_p + F Q L_b - M_p/2 + F Q L_b/2 + \\ H_1 L_c/16 - 3(P+Q)\Delta_2$$

or

$$H_2 L_c/2 = 1.5 M_p - Q L_b + 4.5 F Q L_b + H_1 L_c/16 - 3(P+Q)\Delta_2 \quad 3.5$$

The lateral load H_2 and the lateral deflection Δ_2 can be related by applying the moment-area theorem to the triangular moment diagram shown in Fig. 3.7. It has been shown, that for single story, single

bay frame (12):

$$\Delta_2 = M L_b L_c / 6 EI_b + M L_c^2 / 12 EI_c$$

But considering the model of the frame after the first hinge, shown in Fig. 3.4, the deflection equation relating Δ_2 to moment for single story-two bay frame is one-half as much. Therefore

$$\Delta_2 = M L_b L_c / 12 EI_b + M L_c^2 / 24 EI_c \quad 3.6$$

This is true since by addition of one bay we have doubled the stiffness of the structure. Therefore the deflection due to lateral load is only one-half. From Fig. 3.7:

$$M = H_2 L_c / 4 + 3/2 (P+Q)\Delta_2 \quad 3.7$$

Therefore:

$$\Delta_2 = \frac{\left[\frac{H_2 L_c}{4} + \frac{3}{2} (P+Q)\Delta_2 \right] L_b L_c}{12 EI_b} + \frac{\left[\frac{H_2 L_c}{4} + \frac{3}{2} (P+Q)\Delta_2 \right] L_c^2}{24 EI_c}$$

But since $\psi = \frac{EI_c/L_c}{EI_b/L_b}$

The above equation can be simplified and rearranged to:

$$\Delta_2 = \frac{(H_2 L_c^2)(2\psi + 1)}{96 EI_c/L_c - 6 L_c (P+Q)(2\psi + 1)} \quad 3.8$$

Now by substitution of equation 3.8 into equation 3.5:

$$\frac{H_2 L_c}{2} = 1.5 M_p - Q L_b + 4.5 F Q L_b + \frac{H_1 L_c}{16} - 3(P+Q)$$

$$\left[\frac{(H_2 L_c^2)(2\psi + 1)}{96 EI_c/L_c - 6 L_c (P+Q)(2\psi + 1)} \right]$$

or after simplifying and solving for H_2 , gives:

$$H_2 = \frac{1}{L_c} \left(1.5 M_p - Q L_b + 4.5 F Q L_b + \frac{H_1 L_c}{16} \right) \left[2 - \frac{(P+Q)L_c^2(2\psi + 1)}{8 EI_c} \right]$$

Now, the index value for the critical buckling load, defined as

$$P_E = \frac{\pi^2 EI_c}{L_c^2} \quad \text{may be substituted into the above equation.}$$

$$H_2 = \frac{1}{L_c} \left(1.5 M_p - Q L_b + 4.5 F Q L_b + \frac{H_1 L_c}{16} \right) \left[2 - \frac{\pi^2 (P+Q)(2\psi + 1)}{8 P_E} \right]$$

3.9

By applying the condition of neutral equilibrium, if the frame is unstable after the first hinges form, then H_2 is equal to zero. Therefore, from equation 3.9, when $\left[2 - \frac{\pi^2 (P+Q)(2\psi + 1)}{8 P_E} \right] = 0.0$,

H_2 will be zero. Therefore:

$$\frac{\pi^2 (P+Q)(2\psi + 1)}{8 P_E} = 2$$

$$\text{and } (P+Q)/P_E = 16/\pi^2(2\psi + 1) \quad 3.10$$

Now, let us consider the condition of the frame when the second hinge forms at joint M.

The moment caused by gravity loads P , Q and the lateral load H_1 and its respective deflection Δ_1 , is:

$$M_m = Q L_b/3 - F Q L_b + H_1 L_c/24 \quad 3.11$$

The moment caused by lateral load H_2 and its respective deflection Δ_2 is:

$$M_M = H_2 L_c / 6 + 1/3(3P + 5Q)\Delta_2 \quad 3.12$$

Setting the total moment at M, at collapse equal to M_p :

$$M_p = \left[Q L_b / 3 - F Q L_b + H_1 L_c / 24 \right] + \left[H_2 L_c / 6 + 1/3 (3P + 5Q)\Delta_2 \right] \quad 3.13$$

which after simplifying and rearranging gives:

$$H_2 L_c / 2 = 3 M_p - Q L_b + 3 F Q L_b - H_1 L_c / 8 - (3P + 5Q)\Delta_2 \quad 3.14$$

Now, from equation 3.6, $\Delta_2 = \frac{M L_b L_c}{12 EI_b} + \frac{M L_c^2}{24 EI_c}$ and from Fig. 3.7,

$M_E = H_2 L_c / 4 + 1/2(3P + 5Q)\Delta_2$, therefore:

$$\Delta_2 = \frac{\left[\frac{H_2 L_c}{4} + \frac{3}{2} (P + 5/3 Q)\Delta_2 \right] L_b L_c}{12 EI_b} + \frac{\left[\frac{H_2 L_c}{4} + \frac{3}{2} (P + 5/3 Q)\Delta_2 \right] L_c^2}{24 EI_c}$$

Substituting for $\psi = \frac{EI_c / L_c}{EI_b / L_b}$

The above equation may be simplified and rearranged to:

$$\Delta_2 = \frac{(H_2 L_c^2)(2\psi + 1)}{96 EI_c / L_c - 6 L_c (P + 5/3 Q)(2\psi + 1)} \quad 3.15$$

Now by substitution of equation 3.15 into equation 3.14:

$$\frac{H_2 L_c}{2} = 3 M_p - Q L_b + 3 F Q L_b - \frac{H_1 L_c}{8} - 3(P + 5/3 Q)$$

$$\left[\frac{(H_2 L_c^2)(2\psi + 1)}{96 EI_c/L_c - 6 L_c (P + 5/3 Q)(2\psi + 1)} \right]$$

or after simplifying and solving for H_2 , gives:

$$H_2 = \frac{1}{L_c} \left(3 M_p - Q L_b + 3 F Q L_b - \frac{H_1 L_c}{8} \right) \left[2 - \frac{(P + 5/3 Q)(2\psi + 1)L_c^2}{8 EI_c} \right]$$

Now the index value for the critical buckling load $P_E = \pi^2 EI_c/L_c^2$.

is substituted into the above equation:

$$H_2 = \frac{1}{L_c} \left(3 M_p - Q L_b + 3 F Q L_b - \frac{H_1 L_c}{8} \right) \left[2 - \frac{\pi^2 (P + 5/3 Q)(2\psi + 1)}{8 P_E} \right] \quad 3.16$$

Again, by applying the condition of neutral equilibrium, if the frame is unstable after the first hinges form, then H_2 must be equal to zero.

Therefore, from equation 3.16

$$\left[2 - \frac{\pi^2 (P + 5/3 Q)(2\psi + 1)}{8 P_E} \right] = 0.0$$

or

$$\frac{\pi^2 (P + 5/3 Q)(2\psi + 1)}{8 P_E} = 2$$

which simplifies to:

$$\frac{P + \frac{5}{3} Q}{P_E} = \frac{16}{\pi^2 (2\psi + 1)} \quad 3.17$$

Equation 3.10 represents the stability equation when the second hinge forms at K, and equation 3.17 is the stability equation when the second hinge forms at M. Since the stability of a frame is a "total story" phenomenon (13), the average of these two equations will represent the frame stability equation, when the second hinges form at K and M.

Therefore,

$$\frac{1}{2} \left[\frac{(P + Q)}{P_E} + \frac{(P + 5/3 Q)}{P_E} \right] = \frac{16}{\pi^2 (2\psi + 1)}$$

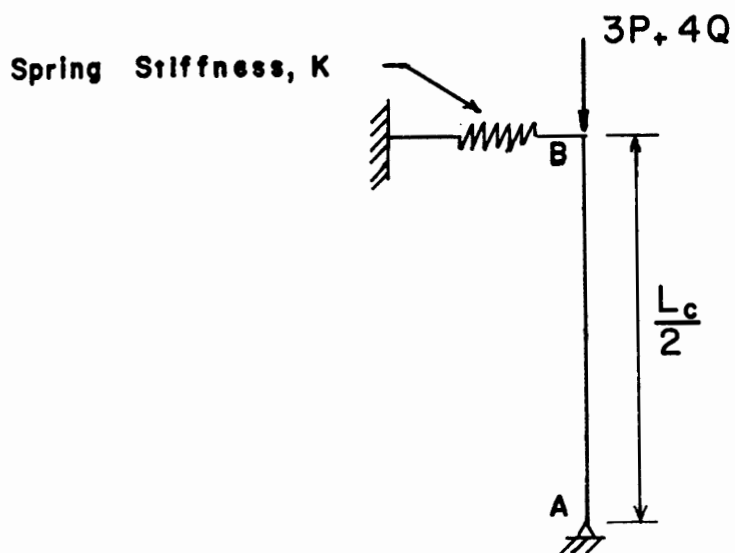
$$\text{or } \frac{P + 1.33 Q}{P_E} = \frac{16}{\pi^2 (2\psi + 1)} \quad 3.18$$

This value of inelastic buckling load for single story two bay frame is 16.7% greater in comparison with one bay frame (12).

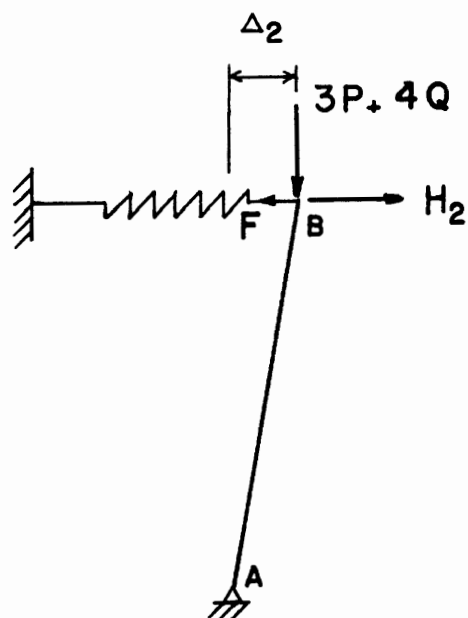
3.6 THE INELASTIC BUCKLING LOAD BY BOLTON'S METHOD

In a paper presented recently by A. Bolton (15) he has shown that the elastic critical buckling load of a structure can be investigated and calculated by using a simple model. The important matter is that whatever is true for this model of the structure is also true for the whole structure.

This model consists of a vertical rigid bar which is freely pivotted at its base A, carries an axial load of $(3P + 4Q)$ (the total load in that story, which should be carried by the frame) at its upper end B, and is supported by a linear spring of stiffness k connected at B, Fig. 3.8a. The vertical bar AB is then displaced by a lateral force of H_2 , causing a deflection of Δ_2 which in effect causes overturning moment ($P-\Delta$ effects) and elastic restoring forces from the linear spring.



(a) The model

(b) The model, after displaced by lateral force H_2 Figure 3.8. The stability model

Then an equation of equilibrium is obtained which is used to solve for the critical load knowing that at this condition the structural stiffness is zero.

It was previously shown that:

$$\Delta_2 = M L_b L_c / 12EI_b + M L_c^2 / 24EI_c \quad 3.6$$

The value of $M = H_2 L_c / 4 + 3/2 (P+Q)\Delta_2$ from equation 3.7 is substituted into the above equation but since the spring assumes a linear characteristic only, the moment will reduce to $M = H_2 L_c / 4$. Therefore:

$$\Delta_2 = H_2 L_c^3 / 96EI_c + H_2 L_c^2 L_b / 48EI_b$$

Substituting for $\psi = EI_c / L_c \sqrt{EI_b / L_b}$ and solving for H_2 :

$$\Delta_2 = H_2 L_c^3 / 96EI_c + \psi H_2 L_c^3 / 48EI_c$$

and

$$\therefore H_2 = \frac{96EI_c / L_c^3}{(2\psi+1)} \Delta_2$$

The spring stiffness k is determined as the force required to cause a unit displacement. Therefore if $\Delta_2 = 1$ is substituted in the above equation:

$$k = \frac{96EI_c / L_c^3}{(2\psi+1)} \quad 3.19$$

Now the equation of equilibrium is obtained by taking moments about A as column AB of Fig. 3.8 is displaced as much as Δ_2 by the lateral force of H_2 :

$$3(P + 1.33Q)\Delta_2 + H_2 (L_c/2) - F (L_c/2) = 0$$

where F = the elastic restoring force in the spring = $k * \Delta_2$
 substituting for $F = k * \Delta_2$ and simplifying

$$H_2 L_c / \Delta_2 = k L_c - 6 (P + 1.33Q)$$

But when axial load reaches its critical value, the structural stiffness H_2 / Δ_2 is zero, therefore

$$0 = k L_c - 6 (P + 1.33Q)$$

or

$$(P + 1.33Q) = k L_c / 6$$

substituting for k from equation 3.19

$$P + 1.33Q = \frac{16EI_c / L_c^2}{2\psi + 1}$$

This equation is now divided by the critical buckling load, $P_E = \pi^2 EI_c / L_c^2$ to result the inelastic buckling load

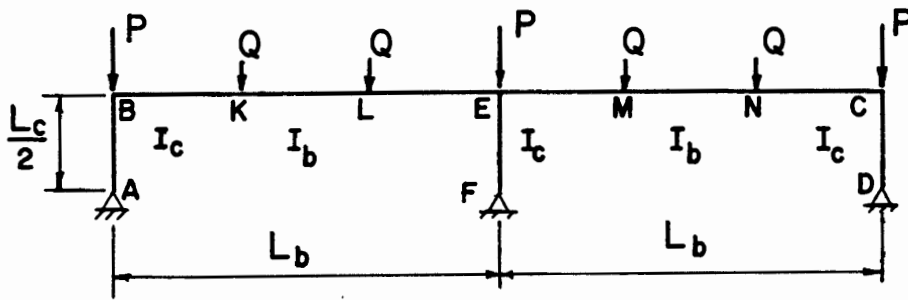
$$\frac{P + 1.33Q}{P_E} = \frac{16}{\pi^2 (2\psi + 1)} \quad 3.20$$

which is the same as the previous solution.

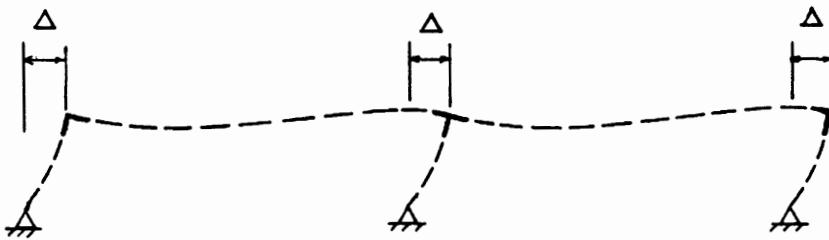
3.7 ELASTIC INSTABILITY OF THE FRAME

Now let us examine the condition under which the frame will buckle elastically, prior to formation of any hinges.

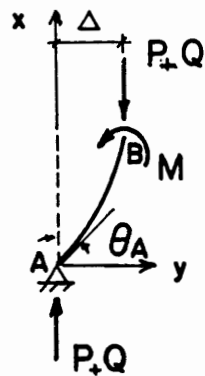
The model frame with its respective deflected shape and the free body diagrams of exterior and interior columns are shown in Fig. 3.9. Of course, knowing ψ_{bottom} and ψ_{top} , by means of Jackson and Moreland nomograph one can find the effective column length factor λ . But for



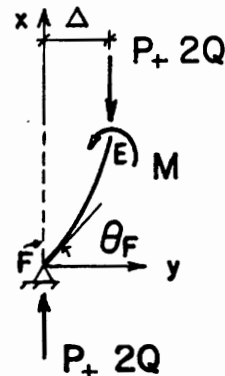
(a) The model frame



(b) The deflected shape of the model frame



(c) FBD of exterior column



(d) FBD of interior column

Figure 3.9. The model frame and freebody diagrams

more accuracy an exact solution is presented in the following.

3.7.1 λ for Exterior Columns. The free body diagram (FBD) of an exterior column is shown in Fig. 3.9c. One may start with the basic differential equation for flexure

$$M = (P + Q)y = -EI_c y''$$

or
$$(P+Q)/EI_c y + y'' = 0$$

Introducing the notation of $k^2 = P+Q/EI_c$, the above equation can be written as:

$$y'' + k^2 y = 0. \quad 3.21$$

The solution of equation 3.21 is

$$y = A \sin kx + B \cos kx$$

Applying the boundary conditions (B.C.):

B.C. 1 at $x = 0, y = 0$

$$\therefore B = 0$$

and $y = A \sin kx \quad 3.22$

B.C. 2 at $x = L_c/2, M_B = -EI_c y''$

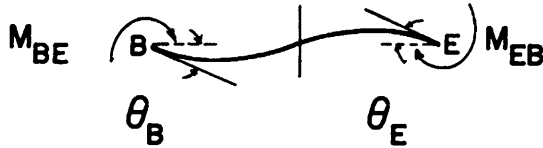
if $y'' = -A k^2 \sin kx$

$$\therefore M_B = EI_c A k^2 \sin kL_c/2$$

substituting for $k^2 = P + Q/EI_c$ and simplifying:

$$A = M_B / (P+Q) \sin kL_c / 2 \quad 3.23$$

using the method of slope deflection for beam BE; and knowing that $\theta_B = \theta_E$ will result:



$$M_B = 6 EI_b / L_b \theta_B \quad 3.24$$

Due to compatibility condition at joint B, it requires that Column $\theta_B =$ Beam θ_B

$$\text{@ } x = L_c / 2, \quad \theta_B = y' = dy/dx$$

From equation 3.22,

$$y' = \theta_B = A k \cos (kL_c / 2)$$

which after substitution into equation 3.24 will result:

$$M_B = 6 EI_b / L_b (A k \cos kL_c / 2)$$

and after substitution into equation 3.23 it can be rewritten as:

$$A = \frac{6 EI_b (A k \cos kL_c / 2)}{L_b (P+Q) \sin kL_c / 2}$$

or

$$\frac{6 k EI_b}{(P+Q)L_b} = \tan kL_c / 2 \quad 3.25$$

now substituting for $(P+Q) = k^2 EI_C$ and for $\psi = \frac{EI_C/L_C}{EI_b/L_b}$ into equation 3.25 it may be shown that:

$$(kL_C/2)\tan(kL_C/2) = 3/\psi \quad 3.26$$

which is the stability equation for the exterior columns.

For example, if $\psi = 2$; substituting into equation 3.26:

$$(kL_C/2)\tan(kL_C/2) = 3/2 = 1.5$$

Now by trial and error solution, one may find $(kL_C/2)$ such that the above equation is equal to 1.5.

$$kL_C/2 = 0.988 \text{ (radians)}$$

or

$$k^2 = \frac{0.9761}{(L_C/2)^2}$$

substituting for $k^2 = P_{cr}/EI_C$, (where P_{cr} is the exterior column critical load):

$$\frac{P_{cr}}{EI_C} = \frac{0.9761}{(L_C/2)^2}$$

or

$$P_{cr} = \frac{(0.9761)EI_C}{(L_C/2)^2}$$

Equating the critical buckling load, $P_{cr} = \frac{\pi^2 EI_C}{(\lambda_e L_C/2)^2}$, with above:

$$\frac{(0.9761)EI_C}{(L_C/2)^2} = \frac{\pi^2 EI_C}{(\lambda_e)^2 (L_C/2)^2}$$

will result, λ_e to be equal to 3.18.

A summary of λ_e for variety of ψ values are shown in table 3.1.

3.7.2 λ for Interior Column. The free body diagram of the interior column is shown in Fig. 3.9d. Following the same procedure, as described in the previous section, it may be shown that,

$$A = \frac{M_{EF}}{(P+2Q) \sin kL_c/2} \quad 3.27$$

By condition of equilibrium at joint E,

$$M_{EF} + M_{EB} + M_{EC} = 0$$

and due to symmetry of the frame,

$$\theta_B = \theta_{EB} = \theta_{EC} = \theta_C$$

by using the slope deflection method:

$$M_{EF} = 12 EI_b/L_b \theta_E \quad 3.28$$

Due to compatibility condition at joint E, it requires that:

$$\text{@ } x = L_c/2, \quad \theta_E = y' = d_y/dx$$

or
$$y' = \theta_E = A k \cos kL_c/2$$

which after substituting into equation 3.28 and back substituting into equation 3.27 it can be rewritten as:

$$A = \frac{12 EI_b A k \cos kL_c/2}{L_b (P + 2Q) \sin kL_c/2}$$

TABLE 3.1
 THE EFFECTIVE EXTERIOR AND INTERIOR COLUMN LENGTH
 FACTOR, BY EXACT SOLUTION

ψ	λ_e	λ_i
.05	2.03	2.02
.1	2.07	2.03
.25	2.17	2.08
.5	2.33	2.17
1	2.63	2.33
2	3.18	2.63
3	3.63	2.91
4	4.07	3.17
5	4.46	3.41
6	4.8	3.63
7	5.14	3.87
8	5.45	4.07
9	5.74	4.27
10	6.02	4.46
15	7.26	5.3
20	8.31	6.02
25	9.25	6.67
30	10.10	7.26
35	10.88	7.81

$$\text{or } \frac{12 k EI_b}{(P + 2Q) L_b} = \tan \frac{kL_c}{2} \quad 3.29$$

now, substituting for $(P + 2Q) = k^2 EI_c$ and the value of $\psi = \frac{EI_c/L_c}{EI_b/L_b}$, into equation 3.29, it may be shown that :

$$\left(\frac{kL_c}{2}\right) \tan \left(\frac{kL_c}{2}\right) = \frac{6}{\psi} \quad 3.30$$

which is the stability equation for the interior column.

Again, for example if $\psi = 2$, it will be determined that $\lambda_i = 2.63$.

A summary of λ_i for variety of ψ values are shown in Table 3.1.

3.8 ELASTIC STABILITY EQUATIONS FOR MULTI-BAY FRAMES

For frames where elastic buckling takes place, $H = 0$. Therefore, for the reduced model, before any hinges form, the elastic buckling load may be expressed as $P_{cr} = \pi^2 EI_c / (\lambda L_c)^2$; where λ = effective column length factor, as was determined by exact solution (see Table 3.1).

According to Yura (13), sidesway buckling is a total story characteristic, not an individual column phenomenon. And in this case, since the column axial thrust for every column is the same, the elastic stability equation of this frame can be defined as below:

$$P_{cr} = \frac{1}{3} \left[\frac{2\pi^2 EI_c}{(\lambda_e L_c/2)^2} + \frac{\pi^2 EI_c}{(\lambda_i L_c/2)^2} \right] = \frac{1}{3} \left(\frac{\pi^2 EI_c}{L_c^2} \right) \left[\frac{8}{\lambda_e^2} + \frac{4}{\lambda_i^2} \right]$$

where: λ_e = effective exterior column length factor

λ_i = effective interior column length factor

not, substituting the index for critical buckling load, $P_E = \frac{\pi^2 EI_c}{L_c^2}$,

$$\frac{P_{cr}}{P_E} = \frac{2}{3} \left(\frac{4}{\lambda_e^2} \right) + \frac{1}{3} \left(\frac{4}{\lambda_i^2} \right) \quad 3.31$$

The graphical solution of the above equation, as a function of ψ , is shown by curve A in Fig. 3.10, which represents the elastic stability equation of a two-bay frame.

The elastic stability equation of frames with 3, 4, 10, or in general J number of bays may be found and is summarized in Table 3.2. These equations are all shown graphically in Fig. 3.10. It is important to recognize that curve A' (for an exterior column or single-bay frame) and curve A'' (for an interior column or many-bay frame) represent the lower and upper bounds of the elastic stability equation. As the number of bays increase, the elastic stability equation gets closer and closer to the upper bound, as the effect of two exterior columns diminish.

3.9 STABILITY DOMAINS DEFINED BY THE ELASTO-PLASTIC ANALYSIS

The stability of the reduced model will be presented in a graphical form. The value of the inelastic buckling load, $(P+1.33Q)/P_E$, where $H_2 = 0$ was found in section 3.5 in terms of ψ ,

$$\frac{(P + 1.33Q)}{P_E} = \frac{16}{\pi^2(2\psi+1)} \quad 3.18$$

The above equation, inelastic instability, is plotted as a function of ψ in Fig. 3.11, which is shown by curve B. Also, the elastic stability equation for two-bay frames which is indicated by curve A in Fig. 3.10, is reproduced here in Fig. 3.11 and again is shown by curve A.

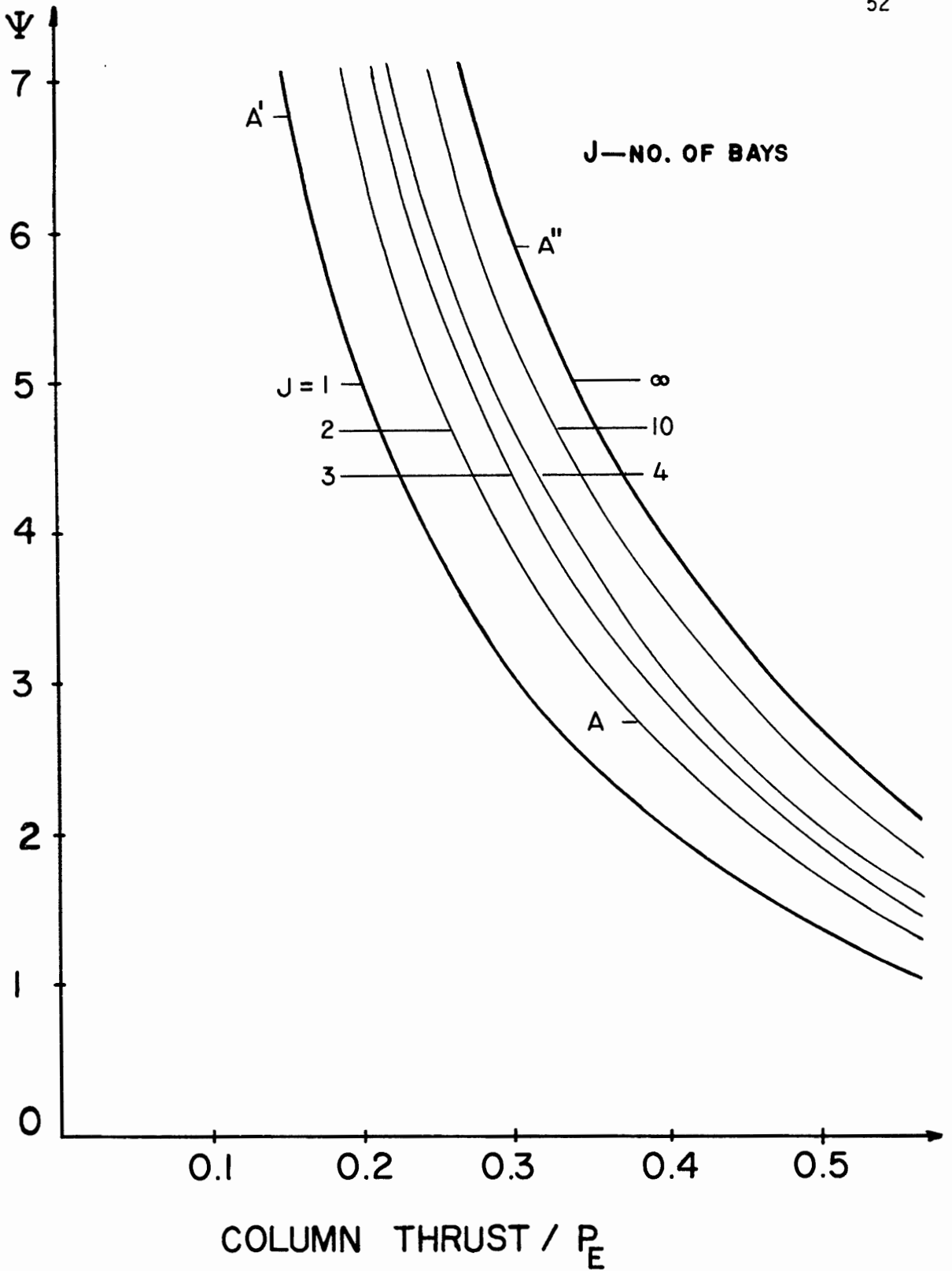

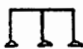
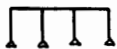
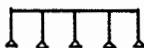
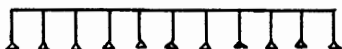
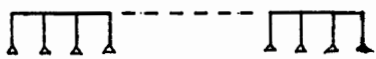



Figure 3.10. The elastic stability equation

TABLE 3.2

THE ELASTIC STABILITY EQUATION FOR FRAMES WITH
DIFFERENT NUMBER OF BAYS

The Elastic Stability Eq., $P_{cr}/P_E = \left(\frac{\text{Exterior}}{\text{Constant}}\right)(4/\lambda_e^2) + \left(\frac{\text{Interior}}{\text{Constant}}\right)(4/\lambda_i^2)$			
No. of Bays J	Exterior Constant	Interior Constant	
1	$(1/2)(2)$	$(1/2)(0)$	
2	$(1/3)(2)$	$(1/3)(1)$	
3	$(1/4)(2)$	$(1/4)(2)$	
4	$(1/5)(2)$	$(1/5)(3)$	
10	$(1/11)(2)$	$(1/11)(9)$	
J	$[1/(J+1)](2)$	$[1/(J+1)](J-1)$	
∞	0	1	

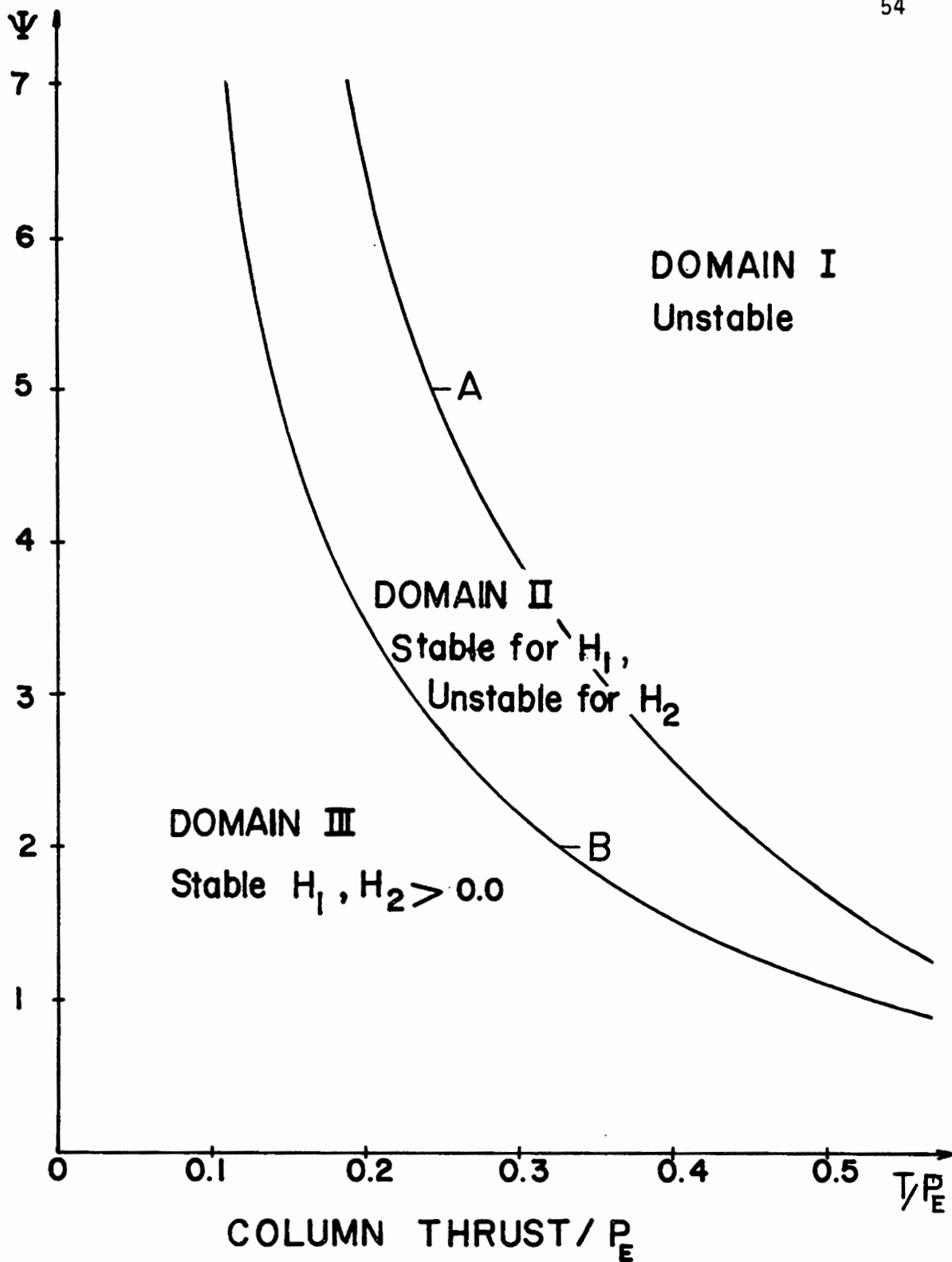


Figure 3.11. The stability domains

Curves A and B divide the total spectrum into three separate domains. Domain I is to the right of curve A which represents the frames that are unstable before any lateral load can be applied. Therefore H_1 and $H_2 = 0$. Domain II, which is the region which lies between curves A and B, represent the frames that are stable only for lateral loads up to H_1 . Therefore $H_2 = 0$.

Domain III, which is to the left of curve B, represents the frames that are stable until a mechanism forms. Therefore H_1 and $H_2 > 0$.

3.10 COMPARISON OF INELASTIC STABILITY EQUATION OF TWO-BAY FRAMES WITH SINGLE-BAY FRAMES

The inelastic stability equation of two-bay frames was determined in the previous section and was plotted graphically as a function of ψ in Fig. 3.11, which is shown by solid curve B in Fig. 3.12. For single-bay frames, the value of the inelastic buckling load as determined in previous studies (12, 24) is $(P + Q)/P_E = 6/(\pi^2(2\psi+1))$ which is shown by dashed curve B in Fig. 3.12.

The comparison of curve B of single-bay with double bay indicates that by adding an additional bay the frame stability has increased about $2\frac{1}{2}$ folds. For example, if flexural rigidity of the columns is the same as the beams, i.e., $\psi = 1$, for two-bay frames resistance to lateral force after the formation of first hinges exists if the column thrusts are less than 54% of the critical buckling load index, P_E . For single-bay frames (24) this value is 20 percent.

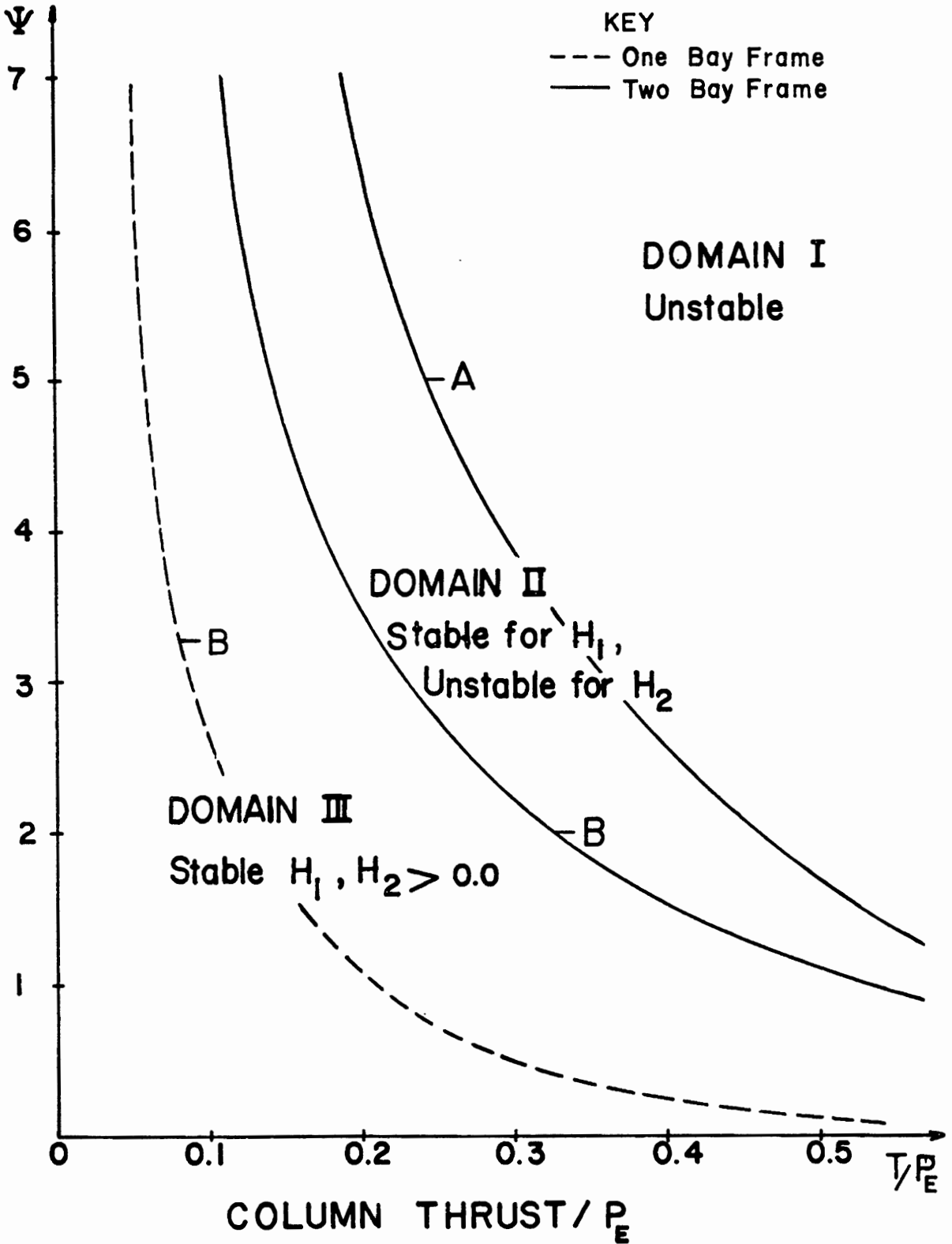


Figure 3.12. Stability domains for one and two bay frames

CHAPTER IV

COMPUTER ANALYSIS

4.1 GENERAL

In this chapter, the stability of unbraced frames will be investigated using a computer program. This program is applied to twenty rectangular model frames with the same overall geometry. Fourteen frames have the same low column reinforcement ratio of 2% but different loading conditions and cross sections. The remaining six frames have the same high reinforcement ratio of 8% but different loading conditions and cross sections.

The column reinforcement ratio (ρ_g) of 2% was chosen to represent a practical value representative of columns in buildings. The maximum value of 8% was chosen to represent the upper limit of column reinforcement according to ACI 318-77, Art. 10.9.1 (4). All beams were assumed to possess a reinforcement ratio $\rho = 1\%$.

4.2 DESCRIPTION OF THE COMPUTER PROGRAM

The computer program used in this investigation is program NONFIX7 (12), which is a version of the computer program NONFIX5, originally developed by Gunnin (16) and later modified by Rad (12). The program is a generalized computational method for nonlinear analysis of planar frames, and takes nonlinear geometry and nonlinear force deformation properties (thrust-moment-curvature, P-M- θ) of the members into account. The P-M- θ relationships for individual members are constructed using a computer program originally developed by Breen (17) which assumes the Hognestad's (18) stress-strain curve relationship for concrete in

compression and an elasto-plastic stress-strain relationship for the steel in tension and compression. The tensile strength of concrete is ignored.

All member cross-sections are assumed to be reinforced symmetrically about the centroid of section, positioned in single layer ($\rho=\rho'$). For the concrete stress-strain curve. The maximum stress was assumed to be $1.0 f'_c$, and the maximum strain was assumed as $\epsilon_u = 0.0038$.

It should be noted that, this program includes the axial thrust-deflection moments caused by the displacements of joints in addition to those caused by nonlinear behavior of the material. Also change in member stiffnesses caused by these moments and the axial thrusts are taken into account.

4.3 PARAMETRIC STUDY OF THE MODEL FRAME

In this section, the nonlinear computer program NONFIX7 is used to study the behavior of twenty different model frames as shown qualitatively in Fig. 2.3 under different loading conditions.

Each beam to column load ratio relates to a particular number of story, n , as shown in Table 4.1. To start, a maximum Q/P' ratio of 0.25 was assumed, which relates to a 3-story building (minimum $n = 3$). For each frame the exterior column axial load, P' , and the interior column axial load, P , were chosen so that the axial-thrust of all columns were equal. Then the gravity loads P' , P and Q , and the lateral load H increased proportionally until frame failure (see Fig. 2.6) occurred.

4.3.1 Frame Description. A dead load of 100 psf was chosen, and three conditions for live load (LL) were selected. Using the Uniform Building Code (UBC), (19) as a guide, for the first condition a light

TABLE 4.1

Q/P', Q/P, Q/T RATIOS FOR VARIOUS NUMBER OF STORIES, n

n	Q/P'	Q/P	Q/T
3	0.25	0.333	0.2
5	0.125	0.143	0.111
7	0.083	0.091	0.077
9	0.063	0.067	0.059
20	0.026	0.027	0.026
30	0.017	0.018	0.017

live load of 50 psf, for the second condition a medium live load of 150 psf, and for the third condition a heavy live load of 250 psf were selected.

The height of the columns (L_c) and the length of the beams (L_b) were 42-in and 84 in respectively. Column and beam sections were reinforced symmetrically with respect to the centroid of the section on two opposite faces in a single layer, throughout the length of the member ($\rho = \rho'$). The thickness of concrete cover, measured from face to center of the nearest steel bar, d_c , was assumed as 0.75 in. A width $b = 6$ in was assumed for both beam and column sections. For the cases of 20 and 30 stories for the beam section, a width $b = 7$ " and for the column sections a width $b = 8$ " and $b = 10$ " were assumed respectively.

The center to center spacing of the frames was assumed to be equal to 84-in, i.e., same as L_b . Grade 60 steel reinforcement ($f_y = 60$ ksi) and the concrete strength $f'_c = 4000$ psi were used. All frames were chosen to approximate a one-third scale factor ($SF = 1/3$).

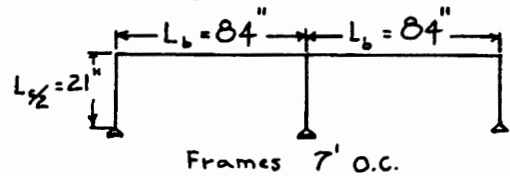
Design of beams and columns of a typical frame is discussed in the following sections. The only variables were Q/P' ratio, loading condition, and column reinforcement ratio.

4.3.2 Design of Beams. All beam sections were designed to carry the gravity load. After the desired loading condition was selected, using equations 9-1 of the ACI-Code (4), the ultimate loads were determined. Then by moment distribution method, moments were calculated and beams were designed. An example of the above design procedure for condition of light live load, i.e., $LL = 50$ psf; is shown below. Note that, an equal reinforcement ratio of one percent, $\rho = 1\%$, for bottom and top

steel layer for all beams was assumed. Therefore:

$$\omega_U = 1.4 (\omega_D) + 1.7 (\omega_L)$$

$$\omega_U = 1.4(100 \text{ psf}) + 1.7(50 \text{ psf}) * 7' = 1.58 \text{ k/ft}$$



from moment distribution method, the maximum moment is, $M_U = 7.72 \text{ k-ft}$.

Effecting the ϕ factor of 0.9 for flexure, will result in

$$M = 7.72/0.9 = 8.58 \text{ k-ft}$$

Using design constants for rectangular beams (21) it may be shown that:

$$M_n = .547 bd^2 = M_U/\phi = 8.58 \times 12$$

setting $b = 6 \text{ in}$, will result in $d = 5.60$

$$h = d + \text{cover (to steel center)}$$

$$h = 5.60 + .75 = 6.35$$

use $h = 6 \text{ in}$.

$$.85 f'_c ab = A_s f_y$$

$$\therefore .85 \times 4 \times a \times 6 = A_s \times 60$$

$$M_n = A_s f_y (d-a/2)$$

$$8.58 \times 12 = A_s \times 60 (5.25-a/2)$$

The above two equations and two unknowns (a and A_s) may be solved.

After a trial and error solution, it was determined that $A_s = 0.36 \text{ in}^2$ was required. By a similar procedure, the beam sections corresponding to other loading conditions were designed.

Table 4.2, summarizes the design value of the beam sections.

4.3.3 Design of the Columns. For design of columns two cases were considered. For case 1, a reinforcement ratio of two percent, $\rho_g = 2\%$, was used. In this case, for each loading condition, four columns corresponding to a 3,5,7 and 9 story buildings were designed, using the ACI Column Design Handbook (20). Also for the medium live load condition, LL = 150 psf, columns for 20 and 30 story frames were designed. For case 2, a maximum $\rho_g = 8\%$ was used. In this case, for each loading condition, two columns corresponding to a 3 and 9 story building were designed.

The slenderness effect of each column was considered using the moment magnifier method, Article 10.11 of the 318-77 ACI Code (4). It consists of multiplying the column end moment by a magnification factor δ . The ACI code equations (10-8) and (10-10) were used to determine this factor. Equation 10-10 is:

$$EI = \frac{(E_c I_g / 2.5)}{1 + \beta_d} \quad 4.1$$

where EI = flexural stiffness of compression member and equation 10-8 is used to calculate the elastic critical buckling load:

$$P_c = \frac{\pi^2 EI}{(\lambda l_u)^2} \quad 4.2$$

where λl_u = effective column length

The above values are then substituted in ACI equation 10-7 to find the magnification factor:

TABLE 4.2
THE SUMMARY OF BEAM SECTIONS

Loading Cond. DL = 100 psf		b (in)	h (in)	d (in)	A_s (in) ²	$\rho = \frac{A_{st}}{bh}$	d'/h
I	LL=50	6	6	5¼	0.36	0.02	0.125
II	LL=150	6	7	6¼	0.48	0.02	0.0968
III	LL=250	6	9	8¼	0.58	0.02	0.0833

The beam section, for 20 and 30 story

Loading Cond. DL = 100 psf		b (in)	h (in)	d (in)	A_s (in) ²	$\rho = \frac{A_{st}}{bh}$	d'/h
II	LL=150	7	7	6.25	0.54	0.02	0.1071

$$\delta = \frac{C_m}{1 - (P_u / \phi P_c)} \geq 1.0 \quad 4.3$$

where: P_u = factored design column thrust

ϕ = strength reduction factor

$C_m = 1.0$ for unbraced frames (4)

The magnification factor is then multiplied by the moment calculated from the moment distribution to define the design magnified column moment,

$$M_c = \delta M \quad 4.4$$

The critical buckling load, P_c , is a function of the effective column length factor, λ , which in effect is a function of flexural rigidity ratio, ψ . Assuming that flexural stiffness (EI) of both column and the beam are equal, for the exterior column

$$\psi_{\text{Botto.}} = \psi_{\text{Top}} = \frac{EI_c / (L_c)}{EI_b / L_b} = 2$$

which results in $\lambda_e = 1.59$ for the full model that possesses column length = L_c ; or $\lambda_e = 3.18$ for half model that possesses column length = $L_c/2$. For interior column, $\psi = \frac{EI_c / (L_c)}{2EI_b / L_b} = 1$ which results in

$\lambda_i = 1.31$ for the full model, or $\lambda_i = 2.63$ for the half model.

These values were found by the exact solution as described in section 3.7. ACI Column Design Handbook (20) was used in the design of column sections.

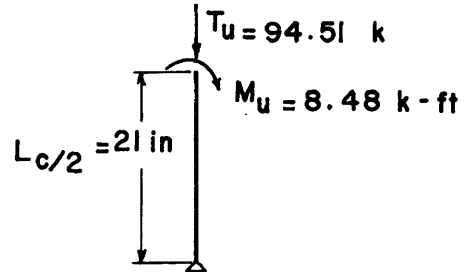
As an example, consider the condition of DL = 100 psf and LL = 150 psf, for a 7 story building ($Q/T = 0.077$). This condition, will result

in a factored column axial thrust of $T_u = 94.51$ k and a column end moment 8.48 k-ft. As mentioned before, $\rho_g = 2\%$ and 8% were desired. A trial and error procedure for $\rho_g = 2\%$ will be described below.

$$b = 6 \text{ in}$$

$$\text{Trial } h = 8 \text{ in}$$

$$r = \left(\frac{I_g}{A_g}\right)^{1/2} = \left(\frac{256}{48}\right)^{1/2} = 2.3 \text{ in}$$



$$\frac{k l_u}{r} = \frac{3.18 * 21''}{2.3 \text{ in}} = 29 > 22 \text{ (ACI Code 10.11.4.2), (4)}$$

\therefore Slenderness must be considered.

Now substituting into equation 4.1,

$$EI = \frac{(3605 \text{ ksi} * 256 \text{ in}^4 / 2.5)}{1 + 0.35} = 273446. \text{ k-in}^2$$

and the elastic critical buckling load using equation 4.2 is:

$$P_c = \frac{\pi^2 * 273446.}{(3.18 * 21'')^2} = 609 \text{ kips}$$

Substituting in equation 4.3 the magnification factor is determined as:

$$\delta = \frac{1}{1 - (94.51/0.7 * 609)} = 1.28$$

$$M_c = (1.28)(8.48 \text{ k-ft} * 12'') = 130.75 \text{ k-in}$$

$$e = 130.75 \text{ k-in} / 94.51 \text{ k} = 1.38 \text{ in}$$

$$e/h = 1.38 \text{ in} / 8 \text{ in} = 0.17$$

Using the ACI Column Design Handbook (20), entering $e/h = 0.17$ and

$\rho_g = 0.02$, $\phi P_n/A_g$ is read:

$$\phi P_n/A_g = 94.51k/A_g = 2.0$$

$$A_g = 47.26 \text{ in}^2$$

$$\therefore h = 47.26/6 = 7.88 \quad \text{v.s. trial } h = 8 \text{ in}$$

By a similar procedure, all the columns for the various loading conditions were designed. Table 4.3 and 4.4 summarize the design value of column sections.

4.3.4 Procedure and Computer Results. The following loading sequence was applied to each frame:

- I. To find the frame ultimate capacity under gravity load only, gravity loads P' , p and Q were proportionally increased until frame failure occurred. The Q/P' ratio relates to the particular number of story of that frame.
- II. Based on the ACI Article 9.2.2 (4), gravity loads P' , P and Q were proportionally increased until 75% of the frame ultimate capacity (under gravity loads only) was reached. The gravity loads were held constant as the lateral load H was applied and increased until frame failure occurred.

The computer output consists of an echo print of input data, along with the results. The results are nodal x and y displacements, nodal rotation, member axial forces, moments, and reactions.

From the computer output, for each frame two relationships were examined: (1) the exterior column load - moment relationships (P' - M) for joints B , K , L and E_w ; and (2) the lateral load moment relation-

TABLE 4.3

THE SUMMARY OF COLUMN SECTIONS, $\rho_g(\text{col.}) = 2\%$

Loading Cond. DL = 100 psf	n	b (in)	h (in)	ρ_g	δ
LL=50 psf	3	6	5.5	0.02	1.22
	5	6	5.75	0.02	1.40
	7	6	6.25	0.02	1.47
	9	6	6.5	0.02	1.59
LL=150 psf	3	6	7	0.02	1.15
	5	6	7.5	0.02	1.23
	7	6	8	0.02	1.28
	9	6	8.75	0.02	1.28
	20	8	14	0.02	1.1
	30	10	17	0.02	1.07
LL=250 psf	3	6	8.25	0.02	1.11
	5	6	8.75	0.02	1.18
	7	6	10	0.02	1.18
	9	6	11.5	0.02	1.15

TABLE 4.4
 THE SUMMARY OF COLUMN SECTIONS, $\rho_g(\text{col.}) = 8\%$

Loading Cond. DL = 100 psf	n	b (in)	h (in)	ρ_g	δ
LL=50 psf	3	6	4.50	0.075	1.49
	9	6	5.75	0.080	2.15
LL=150 psf	3	6	5.50	0.080	1.36
	9	6	7.00	0.080	1.76
LL=250 psf	3	6	6.50	0.080	1.27
	9	6	8.50	0.075	1.47

ships (H-M) for joints B, K, L, E, M, N and C. From the P'-M relationships, it was determined whether the plastic hinges form in the beam or column at corners E and C.

The most useful plots are the H-M curves, which is used to study the inelastic behavior of the frames. From these curves the level of lateral load (H_1) causing the first hinges at corners E_w and C, and the level of lateral load (H_2) causing the second hinges at K and M to produce a combined mechanism were determined.

For some particular cases, the lateral load-deflection relationship (H- Δ) were studied. The H- Δ relationship does give some idea about the level of lateral load (H_2) but not as accurately as the H-M response (14).

The response of each individual frame was studied by plotting a set of (H-M) curves for corners B, C and E and joints K, L, M and H. Each of these sets is identified by a different Q/P' ratio (n stories), and were plotted by using a Tektronix 4051 plotter. As an example, let us consider the behavior of the frames in medium loading condition (DL = 100 psf, LL = 150 psf) and column $\rho_g = 2\%$ which are shown in Fig. 4.1 and 4.2. It appears that the curves essentially consist of two approximately linear parts which are connected together by a curved segment. The bending moment capacity for a particular condition is M_p and is shown by a single value. At zero lateral load, the moments are at 75% of frame capacity under gravity loads. With increasing lateral load, the moments at B, C, E and K, L, M, N change almost linearly until the bending moment capacity is reached at E_w and C. The lateral load at this level is denoted by (H_1). As the lateral load

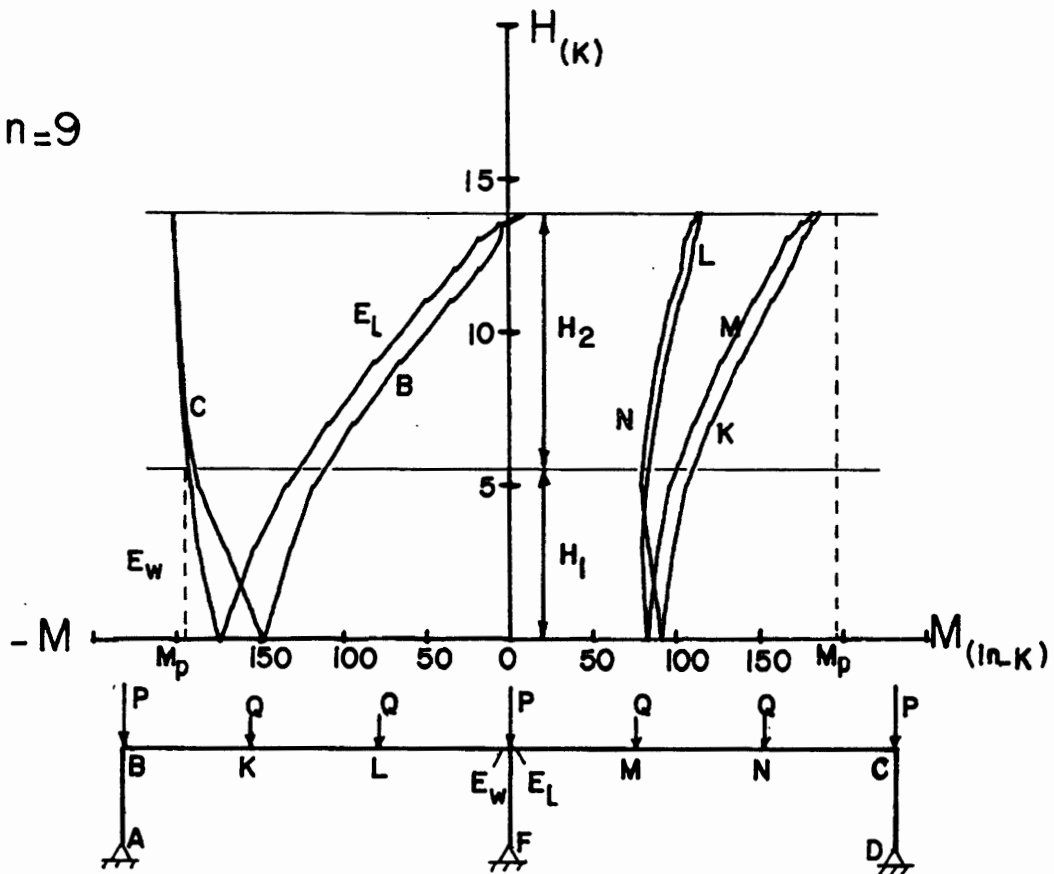
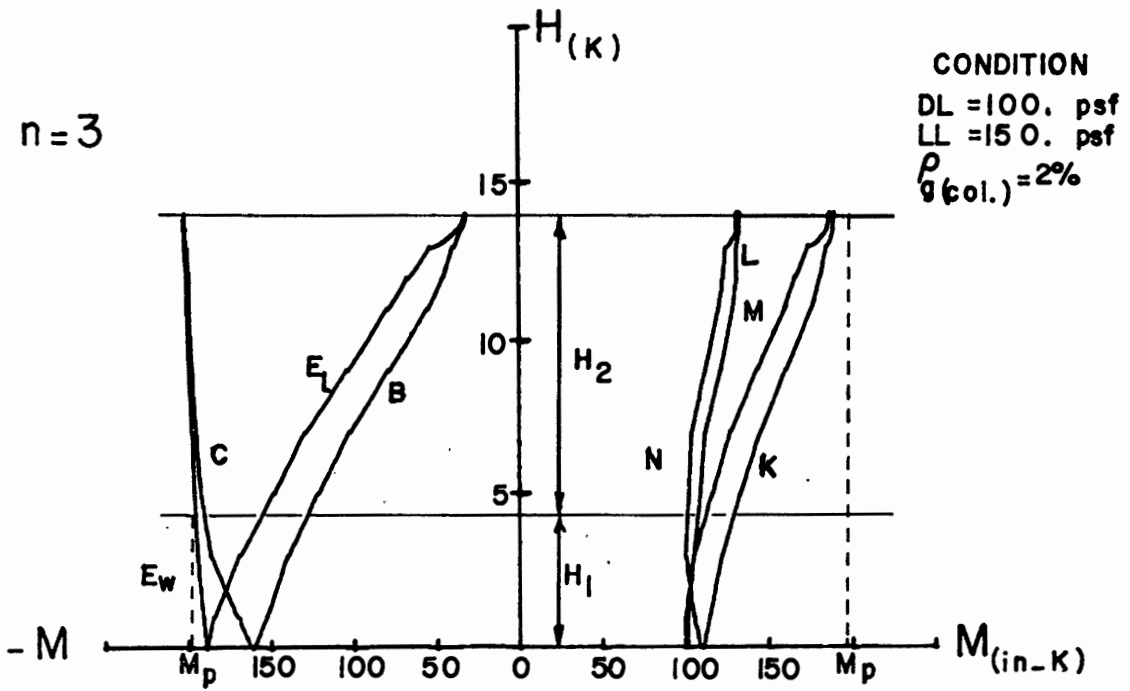
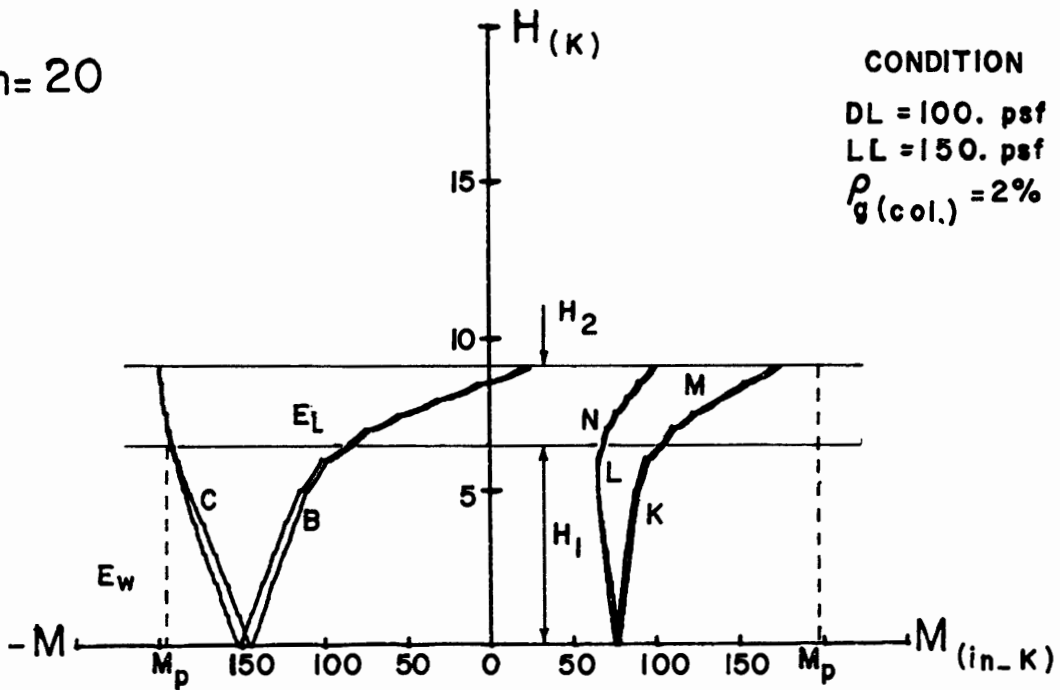


Figure 4.1. Lateral load-moment curves

n=20

CONDITION
 DL = 100. psf
 LL = 150. psf
 $\rho_g(\text{col.}) = 2\%$



n=30

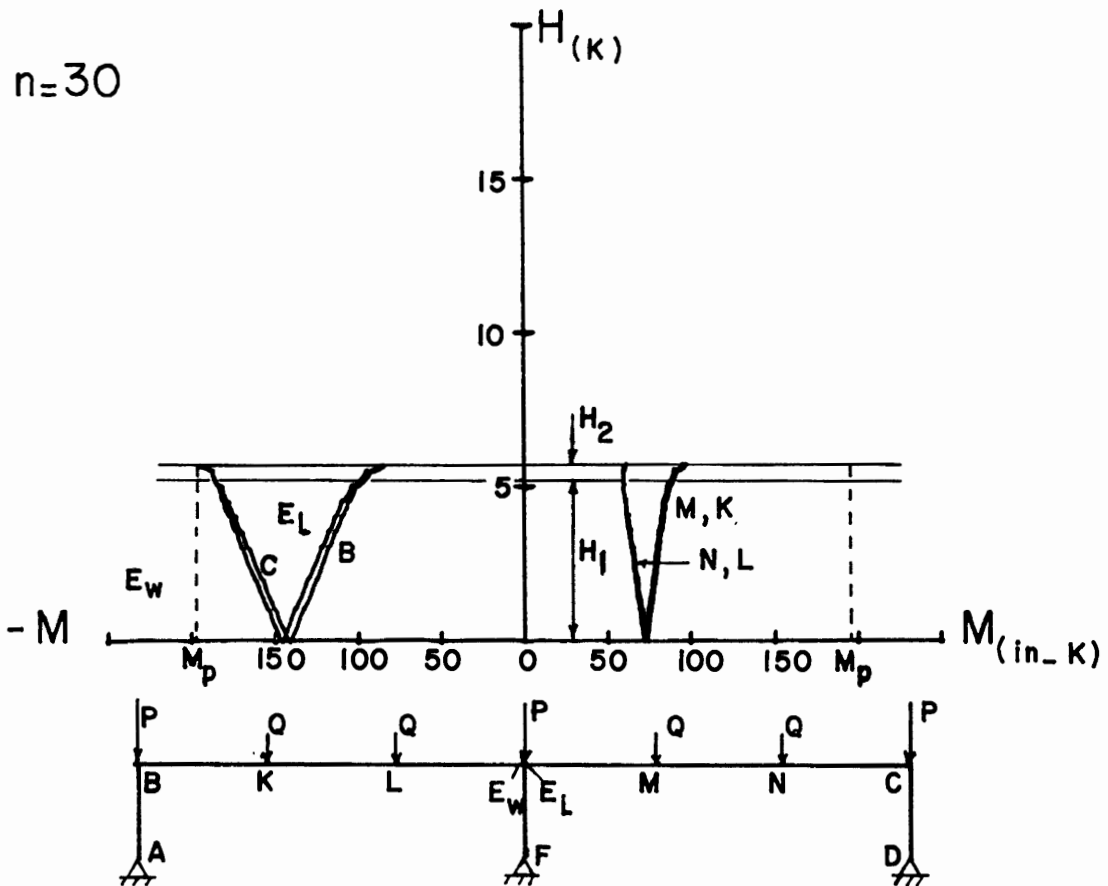


Figure 4.2. Lateral Load-moment curves

increases, the moments at K and M increase more rapidly due to the reduced frame stiffness caused by hinging at E_w and C, while the moments at the later nodes remain unchanged at M_p . Also the moments at B and E_L unwind rapidly to approximately zero. The moments at L and N slightly increase. After the plastic moment capacity M_p is reached at K and M, these locations constitute the second set of plastic hinges. A combined mechanism is then developed and frame is no longer stable failing in a sway motion.

The studies made from behavior of $n = 9$ stories in Fig. 4.1 indicate that in comparison with $n = 3$ stories, the lateral load capacity of frame at the level which first hinges form (H_1) increases but the level at which second hinges form (H_2) decreases.

The behavior of 20 and 30 stories are shown in Fig. 4.2. Their response in comparison with 3 and 9 stories indicate that as the number of stories increases, the lateral load capacity of frame at the level which second hinges form (H_2) to produce a combined mechanism decreases. For the case of 30 stories in Fig. 4.2, H_2 is approximately zero, which indicates the frame after the formation of first hinges becomes unstable and fails.

These differences from 3 to 30 stories are due to the higher column thrust-deflection ($P-\Delta$) moments which are caused by the higher column thrusts in the frame.

CHAPTER V

COMPARISON OF RESULTS BY TWO METHODS

5.1 GENERAL

In this section the frames analyzed in Chapter IV by computer program NONFIX7 are compared with the stability domain of Fig. 3.11. For all the frames, dead load was kept constant at 100 psf, but three live load conditions (1) light LL = 50 psf, medium LL = 150 psf, and heavy LL = 250 psf were selected. Columns in fourteen frames contained reinforcement ratio of 2%, and the remaining six frames had a reinforcement ratio of 8% which is the maximum reinforcement ratio permitted by the ACI Code.

5.2 COMPUTER RESULTS VS. STABILITY DOMAIN ANALYSIS

The computer results for each condition are shown in Tables 5.1 and 5.2. These tables give the column thrust T , lateral load capacity H along with H_1 , H_2 , and the redistribution index $\beta = H_2/H$.

Plots of moment redistribution index β as a function of the number of stories, n , for 3 to 9 story frames with column $\rho_g = 2\%$ and 8% are shown in Fig. 5.1. This figure shows the capacity of the frame after the first hinge decreases as stories vary from 3 to 9. The slope of each line appears to be approximately constant. As loading becomes heavier, the percent of moment redistribution appears to increase slightly. Also for a specific n , β decreases as percent reinforcement varies from 2% to 8%.

To determine the behavior of these frames beyond $n = 9$, β vs. n is plotted for medium loading condition (DL = 100 psf, LL =

TABLE 5.1

SUMMARY OF COMPUTER RESULTS, $\rho_g(\text{col.}) = 2\%$

Cond.	h	Q/P'	T (k)	H (k)	H ₁ (k)	H ₂ (k)	H ₂ /H (%)
(I) LL=50 psf	3	0.250	18.64	8.22	2.75	5.47	66
	5	0.125	31.76	8.27	3.12	5.15	62
	7	0.083	45.20	7.49	3.12	4.37	58
	9	0.063	56.75	7.49	3.43	4.06	54
(II) LL=150 psf	3	0.250	34.79	14.15	4.50	9.65	68
	5	0.125	59.06	14.85	5.03	9.82	66
	7	0.083	83.77	13.79	5.29	8.50	62
	9	0.063	104.77	14.00	5.78	8.22	59
	20	0.026	283.53	9.10	6.47	2.63	29
	30	0.017	428.90	5.83	5.32	0.51	9
(III) LL=250 psf	3	0.250	51.33	19.25	4.80	14.45	75
	5	0.125	86.80	20.60	6.40	14.20	69
	7	0.083	118.77	22.11	7.84	14.30	64
	9	0.063	151.67	21.62	7.99	13.60	63

TABLE 5.2
 SUMMARY OF COMPUTER RESULTS, $\rho_{g(\text{col.})} = 8\%$

Cond.	n	Q/P'	T (k)	H (k)	H ₁ (k)	H ₂ (k)	H ₂ /H (%)
(I)	3	0.250	18.25	8.73	3.30	5.43	62
LL=50 psf	9	0.063	57.47	7.10	3.20	3.90	55
(II)	3	0.250	35.91	12.67	4.35	8.31	66
LL=150 psf	9	0.063	103.37	14.47	6.00	8.47	59
(III)	3	0.250	50.98	19.14	6.40	12.70	67
LL=250 psf	9	0.063	150.03	21.83	8.59	13.20	61

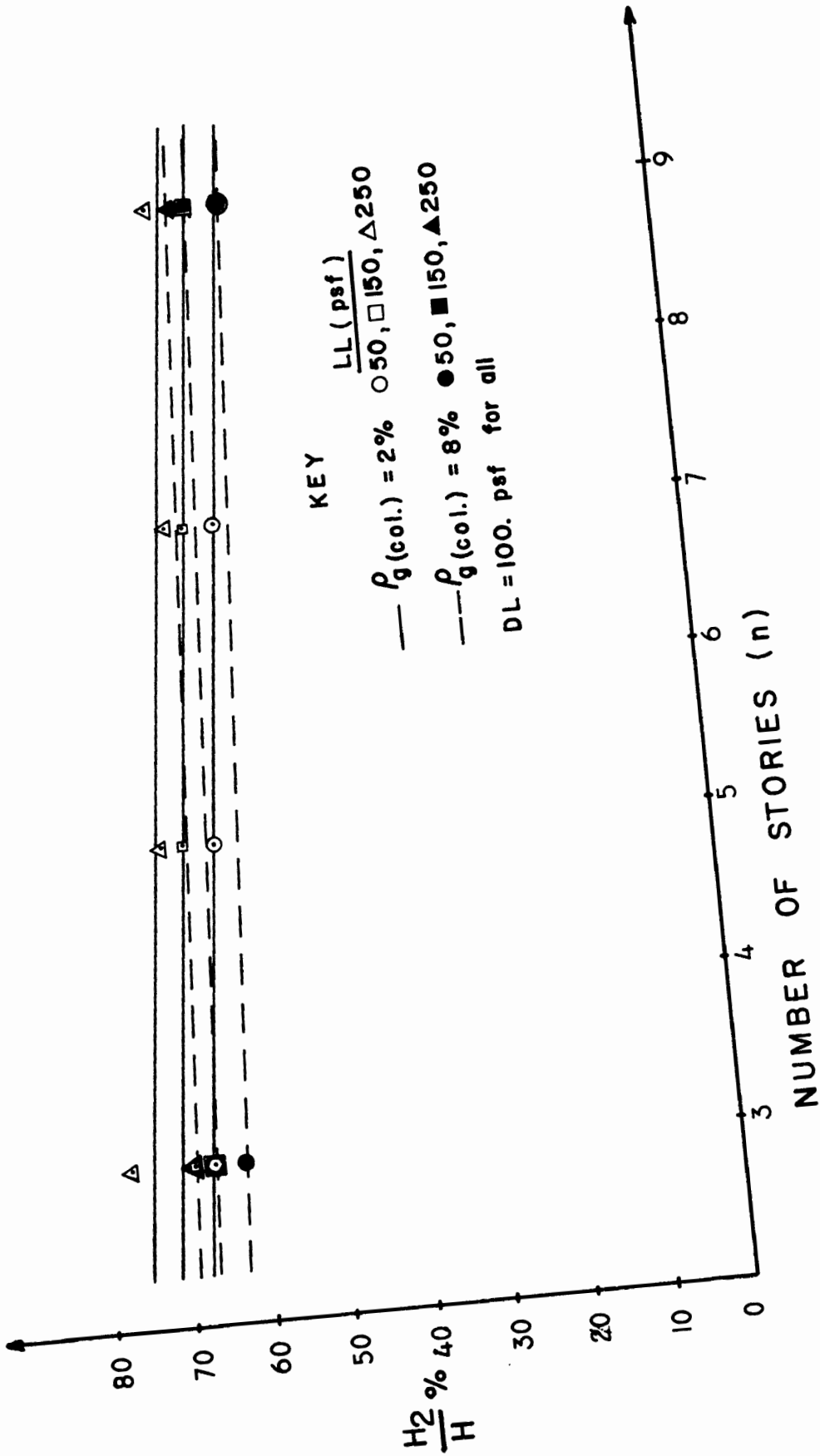


Figure 5.1. Moment redistribution curves

150 psf) with column $\rho_g = 2\%$, as stories vary from 3 to 30, as shown in Fig. 5.2. This figure shows that the capacity of frame after the formation of first hinges decreases with increasing number of stories. Frames higher than 30 stories approach a β of approximately zero, which indicates that they become unstable after the formation of the first set of hinges.

The stability domain of Fig. 3.11 is reproduced here, as shown in Fig. 5.3. Tables 5.3 and 5.4 give the column thrust T , the beam cracked flexural stiffness EI_b , the column flexural stiffness EI_c as determined by ACI Code (4) Equation, the relative flexural ψ , the buckling load index P_E and the ratio of T/P_E .

The values of T/P_E and ψ for 3 and 9 story frames from light to heavy loading with column $\rho_g = 2\%$ to 8% are plotted in Fig. 5.3. All the points fall below curve B in Domain III. This domain relates to frames which are stable until a plastic mechanism occurs. For each specific story, the frame data points tend to group in a cluster form, and as ρ_g increases, this cluster of data tends to shift upward and slightly to the left. Also, with increasing number of stories, the cluster tends to shift upward and slightly to the right.

All data for $n = 3$ through 9 fall in Domain III close to abscissa which indicates substantial stability. This observation was also evident in Fig. 5.1 which indicated high moment redistribution indices for $n \leq 9$.

The data for 20 and 30 story frames are plotted on a reproduction of Fig. 5.3 but drawn to a larger scale, as shown in Fig. 5.4. It shows that for both very small and very large ψ values, the areas contained within Domains II and III become small. Also frames higher

CONDITION
 DL = 100. psf
 LL = 150. psf
 ρ (col.) = 2%

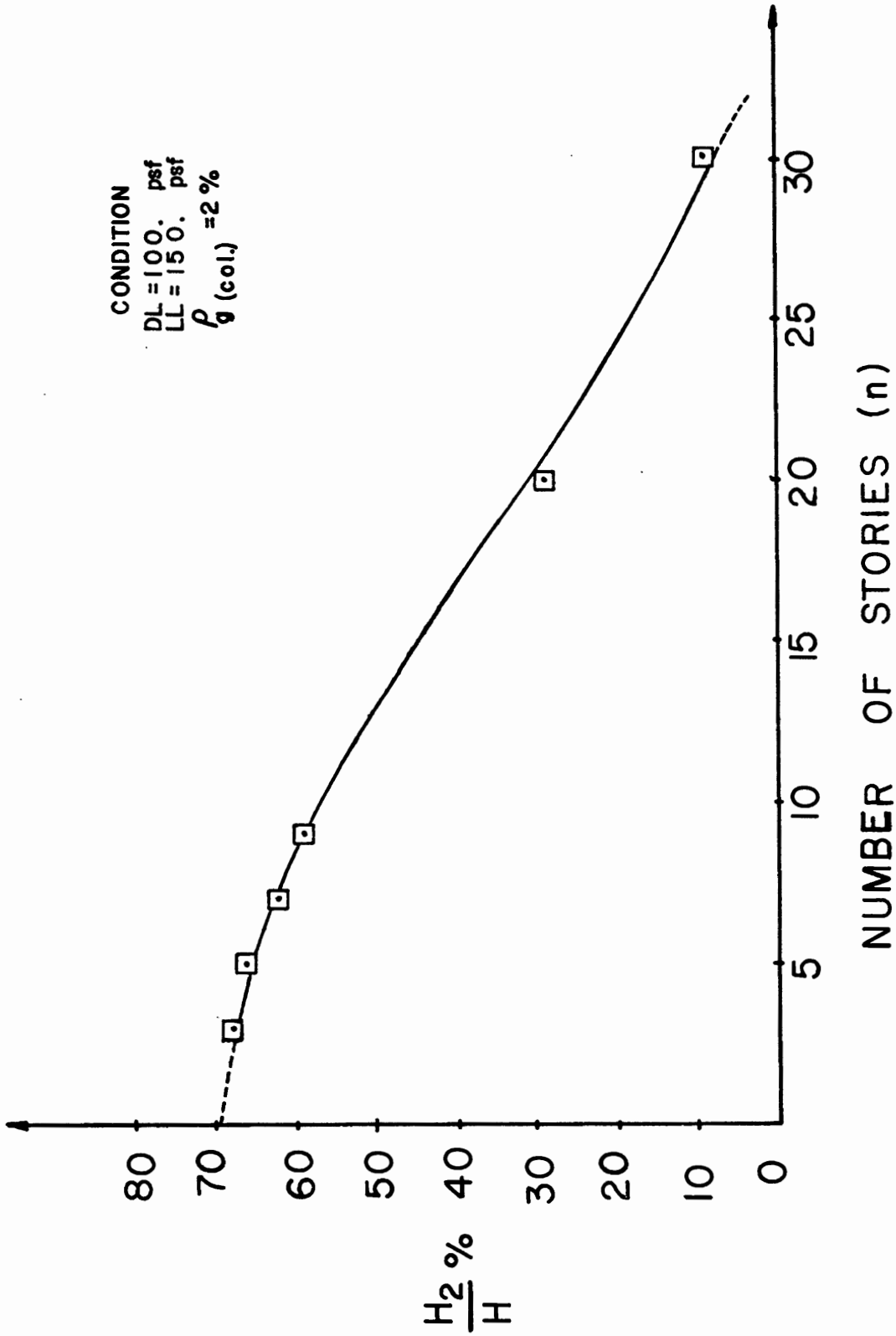


Figure 5.2. Moment redistribution curve

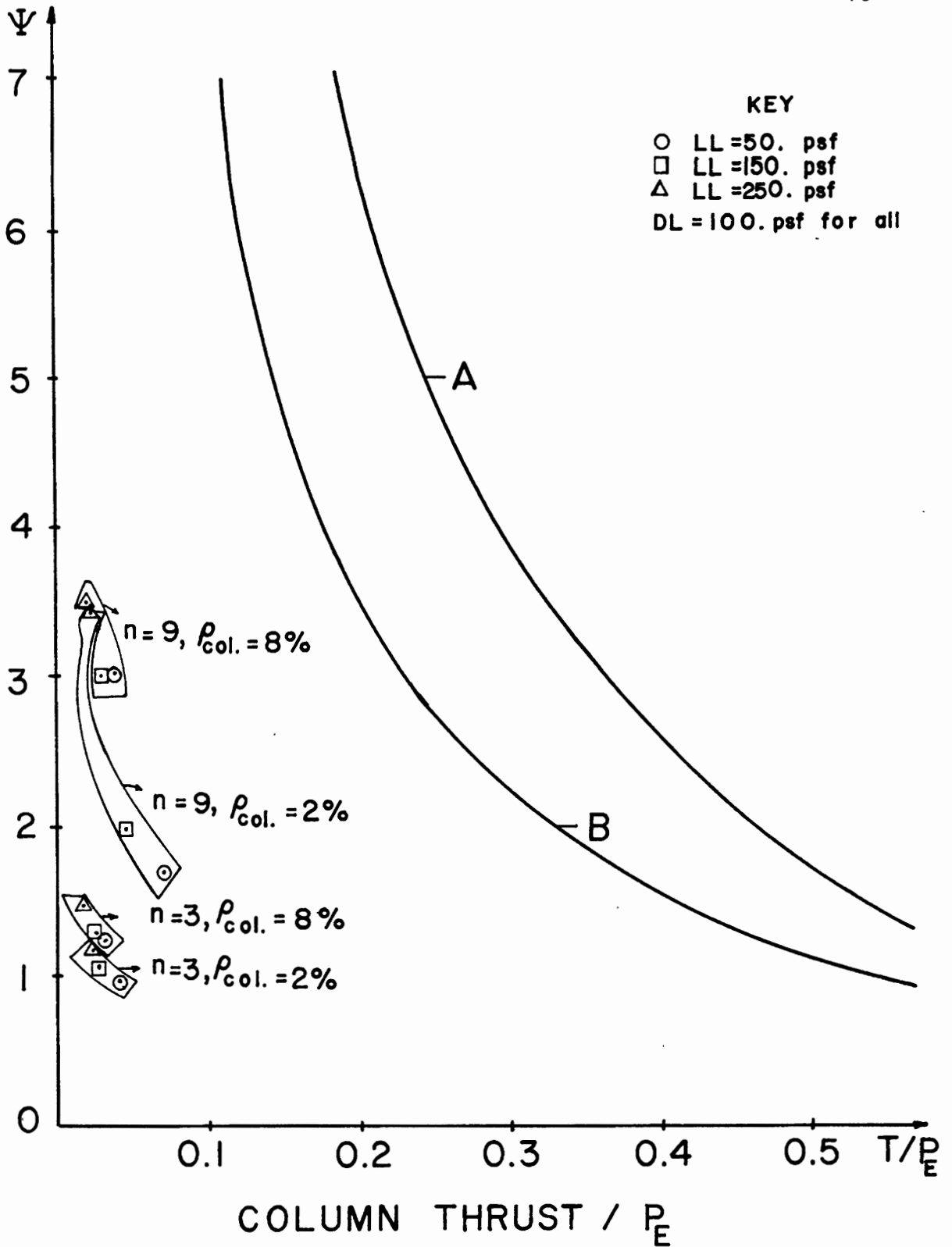


Figure 5.3. The stability domains

TABLE 5.3

COMPARISON WITH STABILITY DOMAIN ANALYSIS, $\rho_g(\text{col.}) = 2\%$

Condition	n	Q/P'	T _(k)	EI _b (k-in ²)	EI _c (k-in ²)	ψ	P _E (k)	T/P _E
(I) LL=50 psf	3	0.25	18.64	175300	84300	0.96	472	.04
	5	0.125	31.76		98100	1.13	549	.06
	7	0.083	45.20		130100	1.48	728	.06
	9	0.063	56.75		148400	1.69	830	.07
(II) LL=150 psf	3	0.25	34.79	424300	228100	1.07	1276	.03
	5	0.125	59.06		286700	1.35	1604	.04
	7	0.083	83.77		354000	1.7	2014	.04
	9	0.063	104.77		421700	1.99	2360	.04
	20	.026	283.53	372800	2856600	15.3	15983	.02
	30	.017	428.9		6573400	35.27	36778	.01
(III) LL=250 psf	3	0.25	51.33	724700	423600	1.17	2370	.02
	5	0.125	86.8		513300	1.42	2872	.03
	7	0.083	118.77		791300	2.18	4427	.03
	9	0.063	151.67		1239000	3.42	6932	.02

TABLE 5.4

COMPARISON WITH STABILITY DOMAIN ANALYSIS, $\rho_g(\text{col.}) = 8\%$

Condition	n	Q/P'	T _(k)	EI _b (k-in ²)	EI _c (k-in ²)	ψ	P _E (k)	T/P _E
(I) LL=50 psf	3	0.25	18.25	175300	107300	1.22	600	.03
	9	0.063	57.47					
(II) LL=150 psf	3	0.25	35.91	424300	271300	1.28	1518	.02
	9	0.063	103.37					
(III) LL=250 psf	3	0.25	50.98	724700	531600	1.47	2974	.02
	9	0.063	150.03					

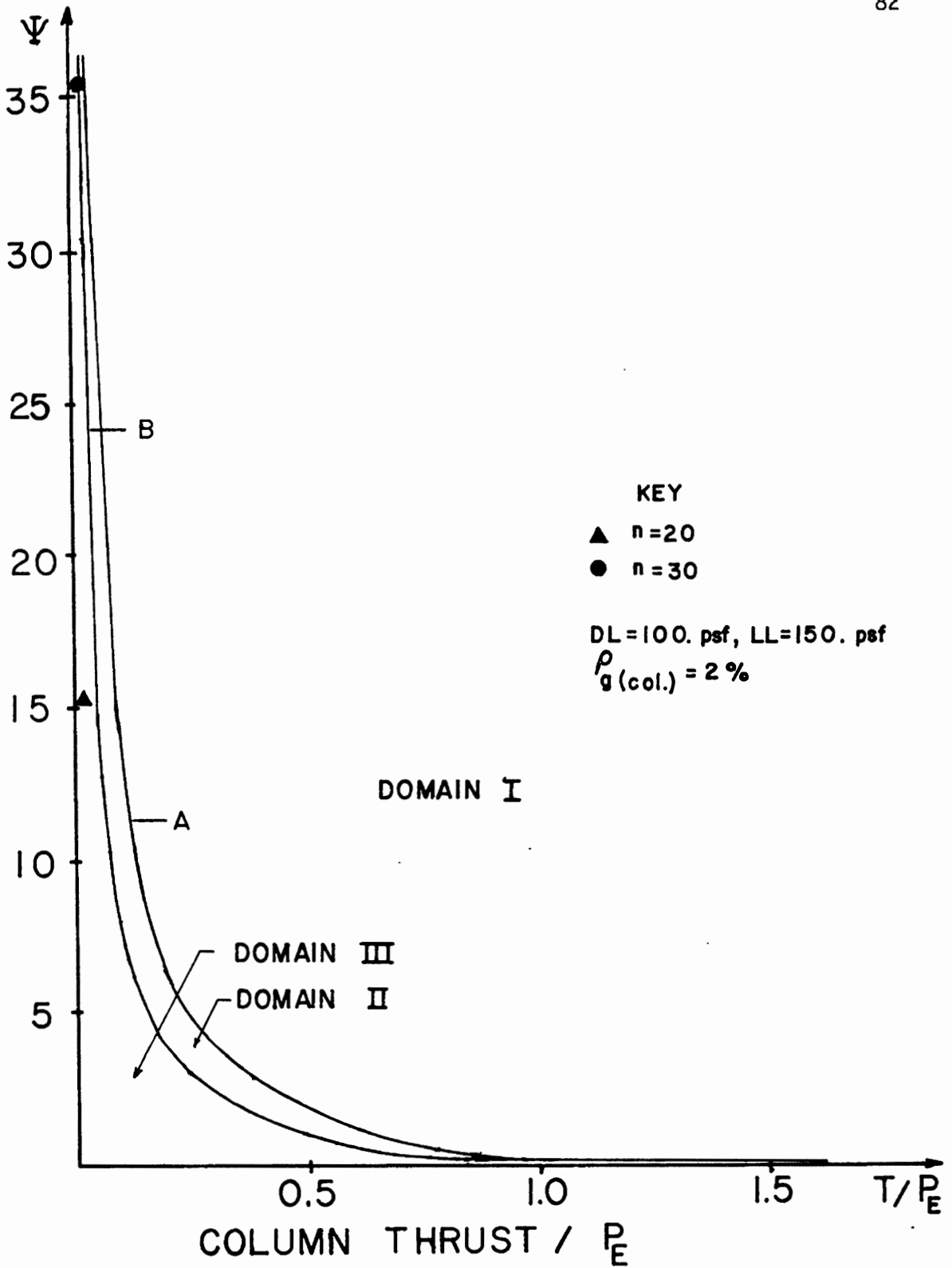


Figure 5.4. The stability domains

than 30 stories tend to fall close to Domain II, which indicates that they become unstable after the first hinges form. This was also evident in Fig. 5.2 which indicated low β for $n = 20$, and β tending to zero as n increased beyond 30.

From the above comparison, it appears that good correlation exists between the elasto-plastic stability domain analysis and the nonlinear computer results.

5.3 SUMMARY OF RESULTS

From the computer results, all 3 to 9 story frames, from light to heavy loading with minimum to maximum column reinforcement ratio, were stable until a plastic mechanism occurred. As the case was examined for 20 to 30 story frames for medium loading with column $\rho_g = 2\%$, results indicated that frames higher than 30 stories are unstable after the first hinges form and thus unable to resist additional lateral load. Therefore, it appears that for frames up to 30 stories, redistribution of moments, which is the essential requirement in limit design, does take place.

Also, these frames were examined using the mathematically derived stability domains. There is good agreement between the results of the two methods of analysis.

Comparison of this investigation with previous investigations on low rise unbraced single-bay frames (14), indicates that by addition of a bay, the stability of the frame is considerably increased.

CHAPTER VI

SUMMARY, CONCLUSIONS AND RECOMMENDATIONS

In this investigation, a scale model frame of a typical prototype unbraced reinforced concrete structure was considered. The primary objective of this study was to determine whether ultimate load theory or limit design can be applied to these structures. The behavior of these model frames was investigated by two methods. In the first method, a mathematical solution was used which assumed the members of the frame possess an elasto-plastic moment-curvature ($M-\theta$) relationship, and flexural rigidities of beam (EI_b) and column (EI_c) do not vary along the length of the members.

From this mathematical solution a stability equation was derived; which exhibited the frame stability as a function of the relative flexural stiffness (ψ) and the column thrust/critical buckling load index (T/P_E). The stability equation was also derived by another model described as a column attached to a linear spring which carries the total frame load from which an identical solution was obtained.

In the second method, the computer analysis of the model frames was accomplished by a computer program which takes material and geometric nonlinearities into account. The variable parameters were the loading condition, reinforcement ratio, and different beam-column load ratio which is a function of the number of stories n . A dead load of 100 psf was chosen constant, and three live load conditions as light 50 psf, medium 150 psf, and heavy 250 psf, were selected. Two cases of column reinforcement ratio, as minimum 2% and maximum 8%, were chosen.

Each frame was designed for a particular number of stories (n), for a specific loading condition, and a percent reinforcement. For each of these frames the gravity loads were increased proportionally until 75% of the frame ultimate capacity under gravity loads are reached. Then, while these gravity loads were held constant, the lateral load was applied and increased to failure.

The overall geometry and width of the columns and beams were the same for all of the model frames.

According to this investigation, the following results and conclusions can be presented:

1. The computer study indicated that all frames from light to heavy loading conditions, remained stable until a combined mechanism failure (Type IV) occurred. The variation in live load did not appreciably affect frame behavior.
2. The computer study for 3 to 9 story frames, indicated that as the column reinforcement ratio varied from 2% to 8% they remained in stable position until a combined mechanism failure occurred. The variation in column reinforcement did not appreciably affect frame behavior.
3. Redistribution of moments, which constitutes the basis for limit design, occurred for all frames up to about 30 stories.
4. Comparison of stability equations between unbraced two bay frame and unbraced single-story frame, indicates that the addition of one bay increases the stable domain by 167 percent.
5. Good agreement was observed between the two methods, i.e., the nonlinear computer method, and the elasto-plastic stability

model analysis.

6. It appears that ultimate load theory or limit design may be applied to multibay unbraced reinforced concrete structures up to 10 to 12 stories high, with a moment redistribution index of 50% or better.

The following recommendations are made:

1. The inelastic stability of frames containing three or more bays should be investigated.
2. Behavior of two bay frames representing 10 to 12 story high structures should be investigated experimentally, in order to verify the high moment redistribution index determined analytically in this investigation.

REFERENCES

1. Bach, C., and Graf, O., Experimental Studies on Fixed-Ended Beams, Heft 45, W. Ernst and Sohn, Berlin, Germany, 1920.
2. Kazinczy, G., Plasticity of Reinforced Concrete, Beton and Eisen, Berlin, Germany, Heft 5, Vol. 32, 1933, pp. 74-80.
3. Brumfitt, E., "Inelasticity and Nonlinearity of Structural Concrete," SM Study No. 8, Bibliography 1968-72, Solid Mechanics Division, University of Waterloo Press, Waterloo, Ontario, Canada, 1972, pp. 513-522.
4. ACI Committee 318, Building Code Requirements for Reinforced Concrete, ACI 318-63, ACI 318-71, ACI 318-77, American Concrete Institute Publications, Detroit, Michigan, 1963, 1971, 1977.
5. Code of Practice for the Structural Use of Concrete, BSI, CP110-72, British Standard Institution, London, England, 1972.
6. Technical Norms for the Design of Concrete and Reinforced Concrete Numbers, N & TU 123-55, Gosstrojizdat, Moscow, USSR, 1955.
7. ICE Committee Report, 1958, Ultimate Load Design of Concrete Structures, The Institution of Civil Engineers, Proc., Feb. 1962, Vol. 21, pp. 400-442.
8. Beedle, L. S., Plastic Design of Steel Frames, John Wiley & Sons, Inc., New York, 1958.
9. International Recommendations for the Design and Construction of Reinforced Concrete Structures, CEB, No. 84, 1972.
10. Instructions for the Design of Hyperstatic Reinforced Concrete Structures Allowing for Stress Redistribution, I 123-50, N.I.I.Zh.B, Moscow, USSR, 1961.
11. Danish Engineering Norms for Civil Engineers, Concrete and Reinforced Concrete Structures, DS, 411-49, Danish Standard Institution, Copenhagen, Denmark, 1948.
12. Rad, F. N., "Behavior of Single Story Two-Column Reinforced Concrete Frames Under Combined Loading," Ph.D. Dissertation, The University of Texas, Dec., 1972.
13. Yura, J. A., "The Effective Length of Columns in Unbraced Frames," AISC Engineering Journal, April, 1971, pp. 37-42.

14. Gavin, T. J., "Limit Design of Unbraced Reinforced Concrete Frames," M.S. Thesis, Portland State University, 1977.
15. Bolton, A., "A Simple Understanding of Elastic Critical Loads," The Structural Engineer, Vol. 54, No. 6, June, 1976, pp. 213-218.
16. Gunnin, B. L., "Nonlinear Analysis of Planar Frames," Ph.D. Dissertation, The University of Texas, January, 1970.
17. Breen, J. E., "The Restrained Long Concrete Column as a Part of a Rectangular Frame," Ph.D. Dissertation, The University of Texas, June, 1962.
18. Hognestad, E., "Study of Combined Bending and Axial Load in Reinforced Concrete Members," University of Illinois Bulletin, Engineering Experiment Station Bulletin Series No. 399, November, 1951.
19. Uniform Building Code (UBC), International Conference of Building Officials, Whittier, California, 1979.
20. Design Handbook in Accordance with the Strength Design Method of ACI 318-77, Vol. 2, Columns, American Concrete Institute Publications, SP-17A (78), Detroit, Michigan, 1977.
21. Ferguson, P. M., Reinforced Concrete Fundamentals, John Wiley & Sons, Inc., New York, 1973.
22. Nawy, E., "Cracking and nonlinear Behavior of Reinforced Concrete," Rutgers University, New Brunswick, N.J., SM Study No. 8, Solid Mechanics Division, University of Waterloo Press, Waterloo, Ontario, Canada, 1972, pp. 95-109.
23. ACI Committee 318, Commentary on Building Code Requirements for Reinforced Concrete, ACI 318-71, American Concrete Institute Publications, Detroit, Michigan, 1971.
24. Rad, F. N., and Furlong, R. W., "Behavior of Unbraced Reinforced Concrete Frames," Journal of the American Concrete Institute, ACI Publications, Proc. No. 4, Vol. 77, July-August 1980, pp. 269-278.
25. Rad, F. N., and Gavin, T. J., "Plastic Mechanism Design of Unbraced Low-Rise Concrete Frames," Journal of the American Concrete Institute, ACI Publications, Proc. No. 5, Vol. 77, September-October 1980, pp. 321-328.
26. Sawyer, H. A., Jr., "Design of Concrete Frames by Two Failure Stages," Proc. International Symposium on Flexural Mechanics of Reinforced Concrete, ACI Publications, Detroit, Michigan, SP-12, 1965.